Mon. Not. R. astr. Soc. (1986) **222,** 809–852

The ultraviolet spectrum and interstellar environment of HD 50896★

Ian D. Howarth and A. Paul Phillips† *Department of Physics and Astronomy, University College London, Gower Street, London WC1E 6BT*

Accepted 1986 May 12. Received 1986 May 12; in original form 1986 February 24

Summary. By combining the results from 52 *IUE* spectra of the WN5 star HD 50896 we have constructed a photometrically precise, flux-calibrated, mean high-resolution ($R \approx 10^4$) data set covering the wavelength range 1150–3274 Å. We give measurements of fluxes and widths for all detected emission lines and P Cygni profiles; approximately 25 per cent of the flux emitted in the *IUE* spectral region comes from line emission. Examination of the interstellar lines shows at least five components contributing to the line-of-sight: H I and H II systems at low velocity, a feature at $\sim -30\,\mathrm{km\,s^{-1}}$ (measured with respect to the low-velocity blend), and absorptions at about -75 and $-130\,\mathrm{km\,s^{-1}}$. We use a profile-fitting analysis to estimate column densities for all available ions in each velocity system. Depletions found in the low-velocity H I gas are typical of those found in other sightlines, while remaining systems show evidence of at least some grain destruction; the $-75\,\mathrm{km\,s^{-1}}$ system, in particular, shows an almost total return of material from grains to the gas phase. We interpret the gas-phase abundances in terms of recent models. By examining high-resolution spectra of a further 15 early-type stars seen close to 50896 in the plane of the sky (and mostly members of the loose cluster Cr 121) we are able to discuss the geometry and physical nature of the various absorption systems observed. We attribute the strong lines of highly ionized species seen towards 50896 to an H II region local to that star, and calculate simple models to demonstrate that the observed columns can be reproduced. The results are consistent with the view that at least some WR stars have far-UV radiation fields characterized by high effective temperatures ($\sim 65 \times 10^3$ K). The $-30\,\mathrm{km\,s^{-1}}$ system is interpreted as arising in the wind-blown bubble S308 associated with 50896, while the higher velocity systems (seen towards many of the field stars in addition to 50896) are discussed in terms of the multiple shock structure expected from a single old supernova remnant. We argue that this SNR is at ~0.8 kpc, and is therefore unlikely to be associated with a mooted neutron star companion to 50896, for which we derive a distance of 2–3 kpc.

★Based on material from the *IUE* archive at the Rutherford Appleton Laboratory World Data Centre.

†Present address: Faculty of Science and Technology, Harrow College of Higher Education, Northwick Park, Harrow HA1 3TP.

1 Introduction

HD 50896 (HR 2583, EZ CMa) is one of the brightest Wolf-Rayet stars in the sky. Because of its low reddening, it is a particularly attractive target for UV spectroscopy. Moreover, since 50896 appears to be one of the stronger candidates for a WR+neutron star system (e.g. Moffat 1982), it has been observed extensively by several groups using *IUE*. A comprehensive appraisal of these results is in preparation by Willis *et al.* (1986a).

At an early stage in the analysis of the *IUE* data it became clear that the interstellar spectrum of 50896 was of considerable interest in its own right, with exceptionally strong lines due to H II region species together with high-velocity blueshifted components in a number of ions. HD 50896 is associated with the ring nebula S308 (Sharpless 1959; Johnson & Hogg 1965; Chu *et al.* 1982), and it has been suggested that the high-velocity features arise in the nebula (e.g. Smith, Willis & Wilson 1980). If this interpretation is correct, then an analysis of the absorption spectrum, using simple, well-understood physics, has the potential of providing a powerful probe of the chemistry of the WR atmosphere and of the interaction of the star's wind with the interstellar medium.

The purpose of this paper is to describe some of the available UV data, to provide an analysis of velocities and column densities of material in the line-of-sight, and to discuss the interstellar environment of 50896. The layout is as follows: Section 2 summarizes the data and their reduction; Section 3 contains a description and brief discussion of the stellar spectrum; Section 4 describes the interstellar line analysis; Section 5 reviews the extinction and hydrogen columns towards 50896; Section 6 discusses the depletion of elements from the gas phase in this sightline; Section 7 gives the results from available density diagnostics; Section 8 introduces data for a number of stars close to 50896 in the plane of the sky; and Section 9 uses the results of the preceding sections to present an interpretation of the absorption systems observed. Section 10 summarizes the principal results and conclusions.

2 Observations

At the time when this project was initiated 31 adequately exposed high-resolution ($\Delta\lambda/\lambda \sim 10^{-4}$) *IUE* spectra were available from the World Data Centre archive. We have merged these data into mean SWP (short wavelength prime camera; $\lambda\lambda \sim 1150$–2050 Å) and LWR (long wavelength redundant camera; $\lambda\lambda \sim 1900$–3275 Å) spectra, which form the primary source for the line profile and equivalent-width analyses reported in this paper. Although many more images are now available (principally as a result of variability studies), we give evidence below that the practical limit of signal-to-noise has already been reached in the merged SWP data discussed here, while relatively few interstellar lines of interest fall in the LWR region.

2.1 THE MEAN SPECTRA

A log of the individual images contributing to the mean spectra is given in Table 1. Because we claim rather high accuracy for our equivalent-width measurements, and detect lines not normally seen in *IUE* data (e.g. P II λ1152.8) we describe our data reduction in some detail.

All the spectra were extracted from the geometrically and photometrically corrected two-dimensional GPHOT images using the STAK and TRAK procedures of Giddings (1981a, b), which incorporate the basic features (and notably the centroiding algorithm) of the highly successful STARLINK IUEDR software (Giddings 1983a, b). Although IUEDR represents a substantial enhancement of the earlier programs, in the present context the only disadvantage of STAK and TRAK is that they incorporated less reliable dispersion constants that are now available.

Table 1. Primary data: high-resolution ($R \sim 10^4$) *IUE* images of HD 50896 used in constructing the mean spectra. The spectrograph small entrance apertures (~3 arcsec radius) have ~50 per cent transmission, the large (~10×20 arcsec) 100 per cent transmission.

Image No. (SWP)	Aperture	Exposure time (s)	Image No. (SWP)	Aperture	Exposure time (s)
1335	Sm	480	10114	Lg	70
2860	Sm	360	10115	Lg	130
4065	Sm	840	14109	Lg	360
8853	Sm	540	14137	Lg	120
9061	Sm	223			
9062	Sm	324	(LWR)		
9063	Sm	649			
9064	Sm	649	2538	Sm	360
10086	Lg	300	3602	Sm	360
10096	Lg	300	7811	Sm	319
10097	Lg	60	7812	Sm	480
10100	Lg	224	8774	Lg	180
10101	Lg	149	8782	Lg	480
10102	Lg	79	8783	Lg	240
10103	Lg	420	8784	Lg	209
10110	Lg	240	8790	Lg	210
10112	Lg	70	8791	Lg	600

We return to this point in Section 2.2; for the moment it suffices to note that we achieved a wavelength scale which is *internally* high consistent from spectrum to spectrum by applying a simple scale and zero-point correction to align selected interstellar features at (arbitrarily) their laboratory wavelengths (using *in vacuo* values shortwards of 2000 Å, air wavelengths longwards). Wavelength measurements of interstellar lines (different to those used to align the spectra) all show standard deviations of <0.02 Å, which largely reflects the accuracy with which the line centroids can be located by eye on a single spectrum.

A correction for the well-known problem of overlap of échelle orders (such that the interorder 'background' is never reached across large parts of the image) was made using a method devised by Giddings (1981a), which is similar in spirit to that given subsequently by Bianchi & Bohlin (1983). The success of this method is clear from examination of the spectra; all the saturated P Cygni profiles and strongest interstellar lines lie close to the nominal zero level. We might expect the most severe problems to be evident in the region of the N v P Cygni profile, $\lambda 1240$, where the échelle order in which the enormously strong emission component occurs lies adjacent to that containing the absorption trough. Results from *Copernicus* suggest that the absorption is essentially black (Johnson 1978; Abbott, Bohlin & Savage 1982); in our mean spectrum a small positive residual flux (~5 per cent of the continuum level) remains. Since this is by far the 'worst case' part of the spectrum, we can safely conclude that the zero level is good to better than 5 per cent of the continuum level throughout the spectra.

Corrections for échelle ripple were carried out 'by hand', adjusting the grating constant K (defined in, for example, Ake 1981) on a spectrum-by-spectrum and order-by-order basis. Although at first sight unimportant for an interstellar line analysis based on equivalent-width measurements and profile fitting to rectified spectra, accurate ripple correction is desirable so that regions of overlap between adjacent orders may be correctly weighted and separate spectra merged consistently, as well as to ensure that broad stellar features are accurately recorded.

Each spectrum was mapped on to a uniform wavelength grid at 0.05 (SWP) or 0.1 (LWR) ångstrom intervals, using a triangular filter; wavelength regions common to more than one order were weighted by the corresponding inverse ripple correction factors. Both *IUE* spectrographs have two entrance apertures: large (~10×20 arcsec) and small (~3 arcsec diameter); all the spectra taken in a given aperture were merged using

$$\overline{F_\lambda}=\frac{\sum_i f_\lambda(i)t(i)w(i)H_\lambda(i)}{\sum_i t(i)w(i)H_\lambda(i)},$$

where $t(i)$ is the exposure time of the ith spectrum, $w(i)$ is a weighting factor (the number by which the mean flux in each spectrum must be divided in order to make it equal the average of the mean fluxes in the large-aperture spectra), f_λ is the flux at wavelength λ (in *IUE* flux numbers per second), and $H_\lambda(i)$ is 1 or 0 for good or bad datum points. [Points were flagged as bad if identified as affected by saturation or truncation in the Intensity Transfer Function tables (the ITF is used to linearize the 'density' in the raw images), fiducial marks in the camera systems, 'spikes', or microphonic readout noise.]

The integrated net fluxes obtained in the SWP large and small apertures differ by a factor ~4. However, the S/N ratios in the corresponding merged spectra are indistinguishable, at a value of about 50 (LAp:SAp=0.97). (Signal-to-noise was estimated from the residuals to low-order polynomial fits to selected 'windows' sampling most of the available wavelength range.) We take this as evidence that over much of the image we have reached the limits of accuracy imposed by fixed pattern noise in the *IUE* camera systems, arising from errors in the ITF tables.

Combining the large- and small-aperture results with equal weights gives a final mean SWP data set with a S/N of ≈70; this quadratic improvement confirms that the noise patterns in the corresponding spectra are essentially independent. Without unusual observing procedures (i.e. exposing in different parts of the large aperture to sample significantly different parts of the camera faceplate), we consider this to be the effective limit to signal-to-noise achievable using *IUE* data, pending an improved ITF. Fewer spectra contribute to the LWR mean, whose S/N is therefore rather poorer, varying with wavelength between ~20 and 40.

2.2 VELOCITY SCALE

The interstellar spectrum of HD 50896 shows a wide variety of ionization stages in several velocity systems. Although in the mean spectra the differential velocities of resolved or partially resolved components in a single line can usually be reasonably well determined, experience has shown that errors in the STAK and TRAK dispersion constants can result in velocities measured in widely different parts of a spectrum 'drifting' by up to several 10s of km s^{-1} (e.g. Howarth, Prinja & Willis 1984). Because it is of considerable interest to investigate the possibility of systematic *astrophysical* velocity shifts as a function of, say, ionization potential (see e.g. Smith *et al.* 1984), we reduced and measured several additional recent SWP images. A summary of these observations is included in Table 2.

These more recent data were reduced from the photometrically corrected ('PI') images using IUEDR. In addition to taking advantage of the improved dispersion constants available therein, we were able to take account of image distortions due to departures of the camera header temperatures (unrecorded for the earlier data) from the 'standard' value. The wavelength scaling is therefore rather more reliable than in the GPHOT data, although an absolute zero-point is still not available.

In all the interstellar lines the strongest feature is due to a blend of components near zero velocity. Measurements of this low-velocity feature in the PI data shows that, irrespective of ionization or excitation potential, all ions share the same velocity to within the accuracy of the

Table 2. Supplementary *IUE* images. Low-resolution (spectrophotometric) data have $R\sim 250$. SWP 22789 and LWP 3228 are underexposed (LWP means Long Wavelength Prime camera), while LWR 14800 is heavily overexposed.

Star	Image no.	Resltn.	Ap.	T (s)	Star	Image no.	Resltn.	Ap.	T (s)
HD 50896	SWP 4064	Low	Lg, Sm	9.71, 5.61	HD 51013	SWP 22860	High	Lg	2400
HD 50896	SWP 14136	Low	Lg, Sm	4.80, 1.52	HD 51013	LWP 3230	High	Lg	1800
HD 50896	SWP 14175	Low	Lg, Sm	3.57, 0.70	HD 51036	SWP 22792	High	Lg	2700
HD 50896	SWP 18835	Low	Lg, Sm	3.57, 1.52	HD 51036	SWP 22858	High	Lg	3120
HD 50896	SWP 21806	Low	Lg, Sm	3.57, 3.57	HD 51036	LWR 17387	High	Lg	2160
HD 50896	LWR 3603	Low	Lg, Sm	7.66, 3.57	HD 51036	LWP 3228	High	Lg	1800
HD 50896	SWP 20905	High	Lg	240	HD 51038	SWP 18747	High	Lg	4800
HD 50896	SWP 20908	High	Lg	240	HD 51038	LWR 14797	High	Lg	3300
HD 50896	SWP 20913	High	Lg	240	HD 51283	SWP 19710	High	Lg	135
HD 50896	SWP 20924	High	Lg	240	HD 51283	LWR 14800	High	Lg	900
HD 50896	SWP 20930	High	Lg	240	HD 51283	LWR 15711	High	Lg	90
HD 50896	SWP 20935	High	Lg	240	HD 51285	SWP 17667	High	Sm	2100
HD 50896	SWP 20939	High	Lg	240	HD 51285	SWP 17668	High	Sm	3300
HD 50896	SWP 20945	High	Lg	240	HD 51285	LWR 13927	High	Sm	2100
HD 50896	SWP 20949	High	Lg	240	HD 51285	LWR 13928	High	Sm	3000
					HD 51854	SWP 18748	High	Lg	2400
HD 49233	SWP 18749	High	Lg	2400	HD 51854	LWR 14798	High	Lg	2220
HD 49233	LWR 14799	High	Lg	1800	HD 52596	SWP 19678	High	Lg	720
HD 50154	SWP 18746	High	Lg	3600	HD 52596	LWR 15710	High	Lg	600
HD 50154	LWR 14796	High	Lg	2880	HD 53138	SWP 6560	High	Lg	40
HD 50261	SWP 22791	High	Lg	3900	HD 53138	SWP 6561	High	Lg	80
HD 50261	LWR 17391	High	Lg	2400	HD 53138	SWP 7193	High	Lg	40
HD 50562	LWR 17385	High	Lg	2400	HD 53138	SWP 13564	High	Lg	80
HD 50646	SWP 19709	High	Lg	900	HD 53138	LWR 6196	High	Lg	18
HD 50646	LWR 14801	High	Lg	600	HD 53138	LWR 10197	High	Lg	18
HD 50680	SWP 22793	High	Lg	2700	-22 3880	SWP 22789	High	Lg	3780
HD 50680	SWP 22839	High	Lg	2400	-22 3880	LWR 17389	High	Lg	3300
HD 50680	LWR 17388	High	Lg	1860					
HD 50680	LWP 3216	High	Lg	1800					

measurements (about $\pm 7\,\mathrm{km\,s^{-1}}$). Because *IUE* is unable to provide an accurate absolute velocity scale zero-point, all velocities are henceforth referenced to this low-velocity feature. To convert to LSR velocities probably requires a correction of $\sim +10\,\mathrm{km\,s^{-1}}$ (estimated from Shull 1977, L. J. Smith, personal communication and Hobbs 1984).

2.3 FLUX CALIBRATION

When discussing the stellar spectrum and the interstellar reddening it is useful to have a flux calibrated data set. We are precluded from using a standard calibration (e.g. that of Cassatella, Ponz & Selvelli 1981) because of our non-standard extraction procedures (in terms of the *IUE* standard image processing system), and in particular because of the order overlap correction we have used. Moreover, we are dubious about the fundamental validity of applying a flux calibration to high-resolution *IUE* data which have been extracted without regard to tracking the échelle orders and without a correction for order overlap. Therefore, to convert our mean spectra to absolute fluxes we first smoothed them, using a Gaussian filter of FWHM=6 Å to simulate the *IUE* low-resolution point-spread function, then binned the data at approximately the sampling rate of low-resolution spectra. [These operations, and all other post-extraction data manipulations, were carried out using DIPSO (Howarth & Marslen 1983).] This gives a data set which is directly comparable to *IUE* low-resolution (spectrophotometric) observations; straightforward division by a low-resolution spectrum then yields the required flux calibration. In practice, we used a combination of least-squares polynomial and spline fits to smooth the calibration curve and to interpolate on to the high-resolution wavelength grid.

To construct the calibration we at first used the low-resolution data reported by Nussbaumer *et al.* (1982), but found that their tabulated fluxes do not exactly reproduce their plot of the 50896 spectrum. (This is apparently due to the use of two different extraction programs with slightly different sampling rates; L. J. Smith, personal communication.) In addition, it is not clear that the exposure times they adopted took into account the quantization effects described by Schiffer (1980). For safety, therefore, we sequestered all the low-resolution untrailed *IUE* images of 50896 available in the archive (Table 2), extracted them using IUEDR, and merged the data (large and small apertures, SWP and LWR cameras) using weights proportional to net signal. [The known decrease in sensitivity of the LWR camera with time (Clavel, Gilmozzi & Prieto 1985) has a negligible effect on these spectra.] We then used these data to flux calibrate the high-resolution spectra as described above; the result is shown in Fig. 1. Also shown are S2/68 data, converted to a flux scale consistent with the *IUE* calibration (Carnochan 1982, and personal communication).

Of course, our final fluxes are entirely dependent on the adopted low-resolution database. None the less, we have the considerable advantages of high signal-to-noise and resolution, as well as freedom from saturation. The last point is of importance, since *IUE*'s small dynamic range means that the strongest emission lines in the 50896 spectrum (N V λ1240, He II λ1640) heavily saturate the detectors in otherwise optimally exposed images.

2.4 FIELD STARS

In order to interpret our data in terms of 50896's interstellar environment we examined *IUE* spectra of a number stars seen nearby in projection on the sky (Section 8). These stars were selected on the basis that they be within a 4°×4° box centred on 50896, and that they have

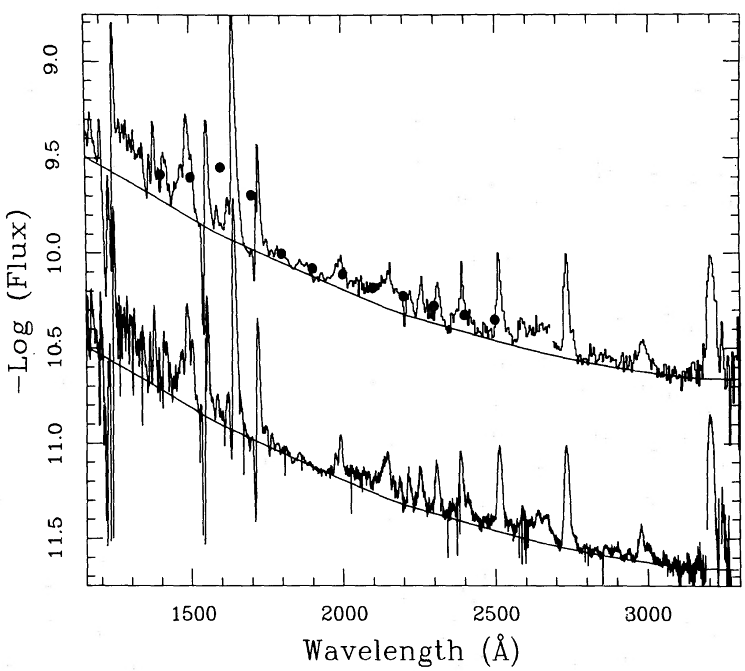

Figure 1. *IUE* spectra of HD 50896. The upper spectrum shows the low-resolution data, and the lower spectrum the high-resolution flux-calibrated data (binned at 0.5 Å and displaced by −1 dex for ease of presentation). In each case the (same) adopted continuum is drawn in. Large dots show the S2/68 results derived using a consistent flux calibration (Carnochan 1982). The unit of flux is erg cm^{-2} s^{-1} Å^{-1}.

high-resolution spectra available in the *IUE* archive. The images, which were all extracted using IUEDR, are listed in Table 2. Where more than one spectrum of a given star was available they were merged, again weighted by net signal, to improve photometric precision.

3 Stellar spectrum

Models of WR atmospheres are just now reaching a stage where quantitative spectroscopic analysis may be contemplated (e.g. Schmutz 1984; Hillier 1984, 1986; Hamann 1985). Although it is not our intention in this paper to present a detailed discussion of the stellar spectrum of HD 50896, the exceptional quality and nature of our data on this star – in many respects a 'standard' WR – make them of particular interest in this context. We therefore give a selection of basic measurements in the hope that they will be of interest to others. Since at least some features show significant variability (Willis *et al.* 1986a) it should be borne in mind that these measurements may not reflect any individual spectrum.

Table 3. Emission-line data. Line identifications taken from Willis *et al.* 1986b. Equivalent widths (in Å) may be calculated from the tabulated data using $EW=-3.55\times10^{-6}\times(\mathrm{Int}-1)\times\mathrm{FWHM}\times\lambda$, where 'Int' is the peak line intensity in units of the continuum level. Five lines near λ1216 (flagged with a '1' in the notes column) have numbers given for fits following correction for a neutral H column of 20.7 dex cm^{-2}.

λ (Å)	FWHM (km s^{-1})	Line flux (erg cm^{-2} s^{-1})	Int.	Notes	λ (Å)	FWHM (km s^{-1})	Line flux (erg cm^{-2} s^{-1})	Int.	Notes
1153.4	1010	1.19(-09)	1.90		1469.7	1290	9.09(-10)	1.82	
1166.7	1180	1.62(-09)	2.07		1475.7	520	1.08(-10)	1.25	
1172.7	1720	1.24(-09)	1.57		1484.8	2090	4.28(-09)	3.46	N IV]
1181.7	1400	5.87(-10)	1.33	1	1492.0	920	8.97(-10)	2.18	
1190.9	610	1.36(-10)	1.18	1; S III	1502.4	2220	2.42(-09)	2.34	
1196.7	850	8.84(-10)	1.84	1	1516.7	980	1.42(-10)	1.18	
1199.3	1430	1.10(-09)	1.62	1; S III	1568.0	1850	4.01(-10)	1.30	
1226.4	520	3.01(-10)	1.49	1	1585.3	1760	5.34(-10)	1.42	
1251.5	970	1.21(-09)	2.08		1595.5	860	9.85(-11)	1.16	
1258.8	840	1.21(-09)	2.25		1603.2	1610	1.49(-10)	1.13	
1263.5	940	1.18(-09)	2.10		1615.9	1030	3.16(-10)	1.44	
1270.3	720	6.71(-10)	1.82		1621.9	920	3.39(-10)	1.53	
1275.6	1220	1.48(-09)	2.08		1737.2	2280	2.70(-10)	1.19	
1285.1	1420	2.12(-09)	2.35		1747.4	1300	1.81(-10)	1.23	N III]
1294.6	700	6.91(-10)	1.90		1765.2	1210	1.45(-10)	1.20	
1299.3	1180	1.27(-09)	1.99		1783.4	2070	1.18(-10)	1.10	
1308.8	1430	1.90(-09)	2.24		1975.4	1240	1.72(-10)	1.30	
1319.7	1570	9.37(-10)	1.56		1991.9	1840	5.45(-10)	1.64	
1329.4	1170	9.92(-10)	1.81		2164.6	920	9.11(-11)	1.26	He II 13→3
1335.8	1010	8.95(-10)	1.85	C II	2187.0	1530	1.88(-10)	1.33	He II 12→3
1340.9	1170	7.57(-10)	1.63		2216.8	1790	2.87(-10)	1.44	He II 11→3
1347.4	910	1.96(-10)	1.21		2254.6	2450	5.44(-10)	1.62	He II 10→3
1361.2	1020	8.86(-10)	1.87		2308.2	1910	5.64(-10)	1.85	He II 9→3
1375.5	1560	2.48(-09)	2.62		2386.6	1730	7.32(-10)	2.28	He II 8→3
1382.6	860	2.60(-10)	1.31		2407.4	2910	1.88(-10)	1.20	
1391.2	910	5.96(-10)	1.68		2412.2	2150	1.30(-10)	1.19	
1398.6	620	1.05(-10)	1.18		2513.1	1790	9.25(-10)	2.50	He II 7→3
1406.7	1030	9.91(-10)	2.03		2588.8	2080	2.60(-10)	1.43	
1410.9	640	1.95(-10)	1.33		2614.4	2750	2.04(-10)	1.26	
1416.9	1740	1.38(-09)	1.86		2639.5	2030	2.32(-10)	1.40	
1427.3	830	3.82(-10)	1.50		2666.1	3100	3.61(-10)	1.41	
1430.9	440	8.68(-11)	1.22		2690.1	1350	3.89(-11)	1.10	
1438.6	890	2.05(-10)	1.26		2734.7	1790	1.21(-09)	3.47	He II 6→3
1445.4	760	3.24(-10)	1.48		2978.3	1870	2.34(-10)	1.49	
1454.7	1690	6.38(-10)	1.43		3204.2	1980	2.67(-09)	6.42	He II 5→3
1463.0	1400	8.40(-10)	1.70						

3.1 EMISSION-LINE FLUXES

The spectrum of 50896 is swarming with emission lines; in the SWP range, in particular, identifying a plausible continuum level is quite difficult, and would be a hopeless task in low-resolution data (this might be a contributory factor to the interpretation by Nussbaumer *et al.* 1982 of a steeply rising UV continuum in the low-resolution spectra of many stars; see Fig. 1). Our adopted continuum is shown in Fig. 1; if anything, it probably still errs on the side of being too high.

In an attempt to overcome as far as possible the problems caused by blending, we measured the emission lines by least-squares fitting of multiple Gaussian profiles (using the ELF routines written by P. J. Storey and integrated into DIPSO). Although a few lines are noticeably abNormal (i.e. non-Gaussian), checks with 'by-eye' measurements on isolated features gave excellent agreement. Where necessary, we snipped out strong interstellar lines which might affect flux measurements, linearly interpolating across the resulting gaps in the data.

Results of the profile fitting are given in Table 3, and a comparison of the observed and synthesized data in a particularly complex part of the spectrum given in Fig. 2. The approach adopted was to add components until a satisfactory match to the observed spectrum was obtained. To some extent, therefore, the results are to be regarded simply as a parameterization of the UV data, although in many cases they should have a reasonably straightforward interpretation in terms of the widths and strengths of individual lines. Common sense, together with inspection of the figures, should suffice to distinguish those features which can be attributed primarily to actual lines or simple blends (e.g. $\lambda\lambda$1285, 1361 etc.) from those which merely match the local shape of the spectrum (e.g. around λ1460).

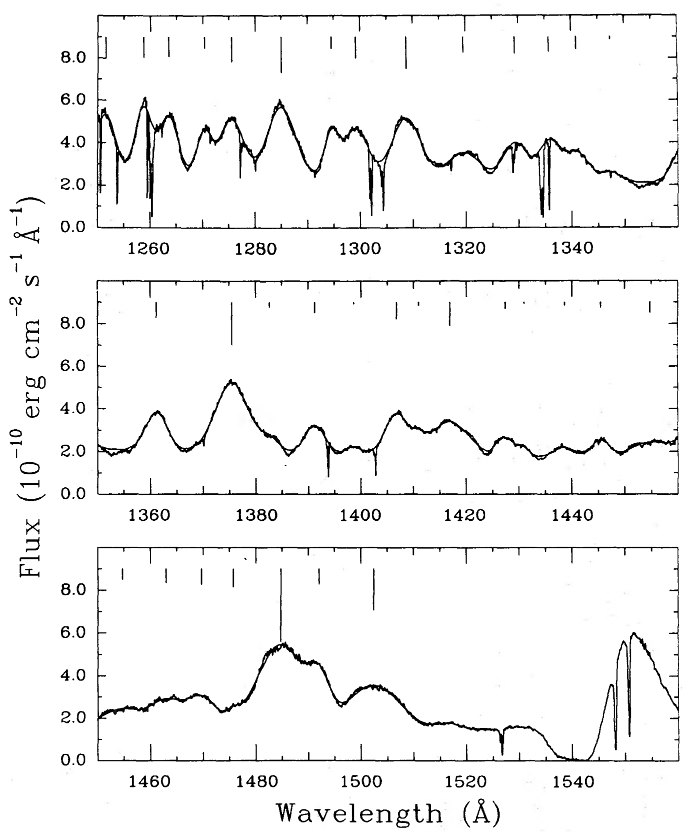

Figure 2. Part of the high-resolution SWP spectrum of HD 50896. The relatively noisy line shows the observations, while the smooth curve (most easily seen where it spans strong interstellar lines) is the Gaussian synthesis of these data discussed in Section 3.1. The vertical ticks mark the centres, and relative strengths, of the fitted Gaussians.

Table 4. P Cygni profiles. Mean wavelengths for doublets are weighted by oscillator strengths; v(max) is the maximum displacement of the absorption feature, measured with respect to the bluewards doublet component; V_0 and V_e, the velocities of central absorption and peak emission, are measured with respect to the mean wavelength. Fluxes are in erg cm^{-2} s^{-1}, wavelengths in Å, velocities in km s^{-1}, and peak intensities are in units of the continuum level.

Line	Mean λ	$v(max)$	V_0	V_e	Flux (Emission)	EW (abs.)	EW (em.)	Peak Int.	'Black' λ
He II	1215.2	-2620	-1780	...	...	...	...	...	...
He II	1640.4	-3200	-1900	-70	1.9(-8)	1.3	-160	16.6	...
C IV	1549.0	-3140	-1680	+470	4.7(-9)	8.5	-34	4.4	4.1Å
N V	1240.1	-2880	-1860	+550	9.5(-9)	8.6	-35	6.6	4.0Å
N IV	1718.6	-2940	-1570	+20	3.5(-9)	4.1	-35	4.4	...

Line identification is a fearsome problem which we have decided not to attack. Table 3 therefore gives only selected identifications, taken from Willis *et al.* (1986b). We have eschewed following their attribution of several features to transitions of Si, given the absence of detectable emission in the resonance lines of Si III and IV. Willis *et al.* report absorption components to a number of lines, including He II 9→3 and 8→3 (but not lower members of the series); we found no evidence for any absorption features save those associated with strong P Cygni profiles (Section 3.2; Table 4) or else of interstellar origin.

Although our improved resolution and signal-to-noise lead to a comparatively reliable definition of the continuum level over much of the UV spectrum, uncertainty in this quantity is still a major source of error. We estimate the emission-line fluxes quoted in Table 3 to be good to probably ~10 per cent in general (or $\sim 10^{-10}$ erg cm^{-2} s^{-1} if larger), but much greater errors may occur if unrecognized blending is important. Nussbaumer *et al.* (1982) and Smith & Willis (1982) have previously reported line fluxes and equivalent widths for 50896, and Willis (1982) has given velocity measurements based on a single high-resolution *IUE* spectrum plus optical data. Tables 3 and 4 include velocities, equivalent widths, and absolute fluxes (not corrected for reddening) for most of the UV lines given in those papers; agreement with these previous results is satisfactory.

For completeness, we note that the total flux in the range 1150–3274 Å is 2.56×10^{-7} erg cm^{-2} s^{-1} in our data (5.56×10^{-7} following correction for an extinction of $E(B-V)=0.1$ using Seaton's 1979 formulae). Subtracting the adopted continuum from the data gives an area of 8.24×10^{-8} (1.78×10^{-7}) erg cm^{-2} s^{-1} (which includes negative contributions from P Cygni and interstellar absorptions); the fits in Table 3 correspond to 5.28×10^{-8} (1.17×10^{-7}) erg cm^{-2} s^{-1}, and the emission components of the P Cygni profiles contribute 3.7×10^{-8} (7.9×10^{-8}) erg cm^{-2} s^{-1}.

3.2 P CYGNI PROFILES

Only four lines in the *IUE* wavelength region clearly show P Cygni profiles, with absorption extending below the adopted continuum (a fifth, less obvious, feature is discussed in Section 3.2.2); results are given in Table 4, and Figs 3 and 4. The data indicate a terminal velocity v_∞ of (-3100 ± 100) km s^{-1}, if we adopt the customary indicator of that quantity, i.e. the maximum velocity observed in absorption. Using the radio flux reported by Abbott *et al.* (1986) then yields a mass-loss rate of

$$\dot{M}=4.7\times10^{-5}\left(\frac{D}{2\,\mathrm{kpc}}\right)^{3/2} F\,M_\odot\,\mathrm{yr}^{-1},$$

where the adopted distance D is discussed in Section 5.4, and F is a factor parameterizing the

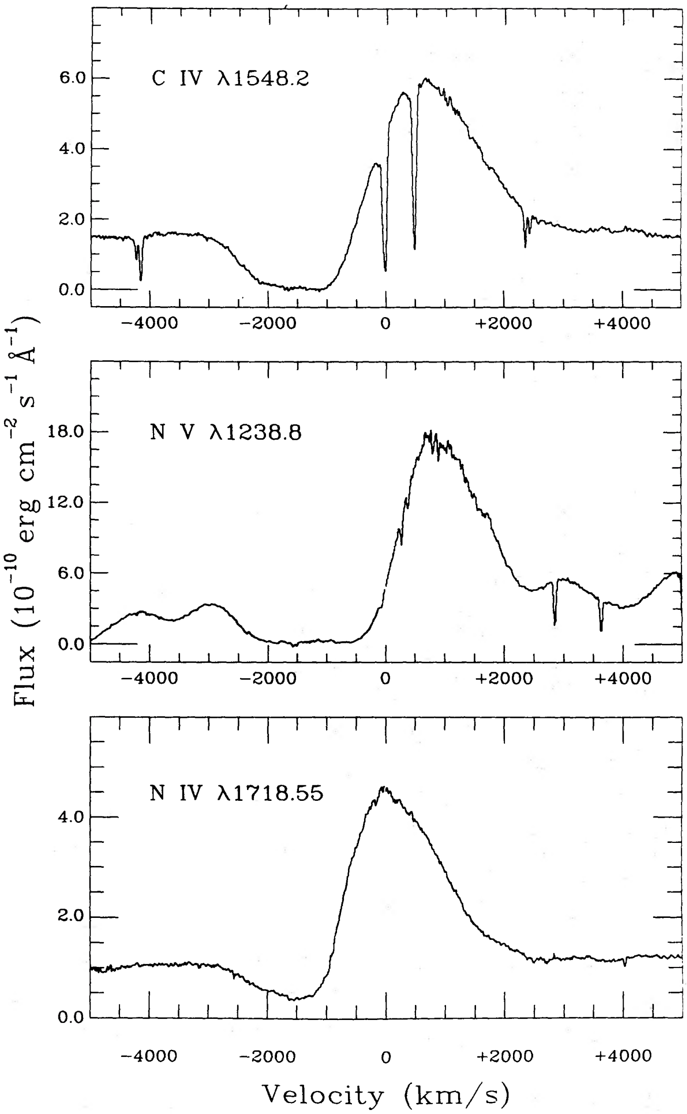

Figure 3. Three P Cygni profiles in the spectrum of HD 50896.

ionization in the radio emitting region ($F=1$ according to Abbott *et al.* 1986, but $F=2.7$ if He is singly ionized; Schmutz & Hamann 1986).

3.2.1 *Saturated profiles*

Both the N V and C IV have absorption troughs which reach essentially zero residual intensity over a range of velocities (Fig. 3); the corresponding values are included in Table 4. (The numbers given correspond to the range of wavelengths over which the residual intensity falls below 0.05.) Lucy (1983) has interpreted such features as a diagnostic of shock amplitudes in the wind; adopting this explanation of the profile shape, we find $v(\text{shock}) \gtrsim 360\,\text{km}\,\text{s}^{-1}$, where the lower limit applies if resonant photons can escape the shock ensemble in the forward direction.

3.2.2 *The λ1215 feature*

Willis (1982) has demonstrated the existence of a positive correlation between the velocity displacement at the centre of a Wolf–Rayet P Cygni absorption and the excitation potential of the

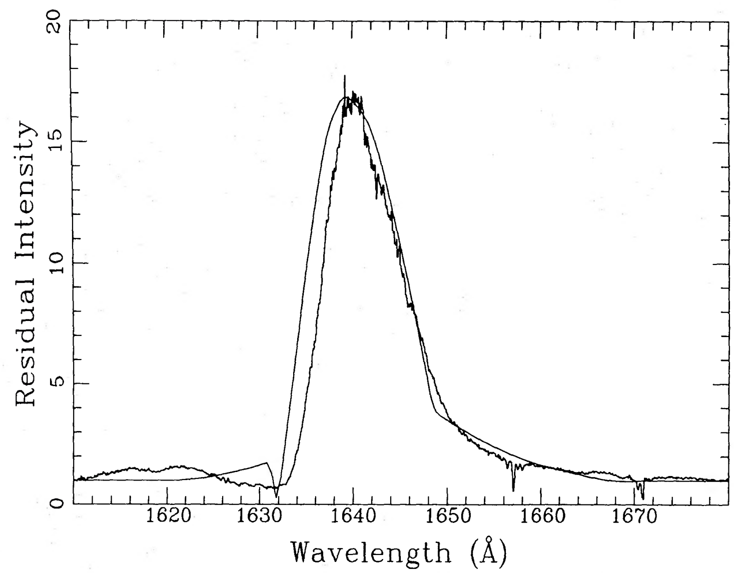

Figure 4. The He II Balmer-α profile in the spectrum of HD 50896. The theoretical profile is from a model by Hillier (1984) corresponding to $\dot{M}=5\times10^{-5}\,M_{\odot}\,\mathrm{yr}^{-1}$.

corresponding lower level in the parent transition. On the basis of this correlation, he identified a weak absorption feature, seen in 50896 (and several other stars) in the violet wing of interstellar H Lyman-α, as due to He II λ1215.2 rather than H I λ1215.7.

In fact, the absorption feature appears to extend to significantly shorter wavelengths in 50896 than identified by Willis, who gave a central velocity, V_0, of $-1276\,\mathrm{km\,s^{-1}}$. Fig. 5 shows the mean spectrum in this region, both as observed fluxes and corrected for an interstellar neutral hydrogen column of 20.7 dex cm^{-2} (see Section 5). From this figure we estimate $v(\mathrm{edge})=-2620\,\mathrm{km\,s^{-1}}$ and $V_0=-1780\,\mathrm{km\,s^{-1}}$. The latter value is in excellent agreement with that expected for a resonance line on the basis of Willis' correlation ($V_0=-1740\,\mathrm{km\,s^{-1}}$), but is more than 600 km s^{-1}

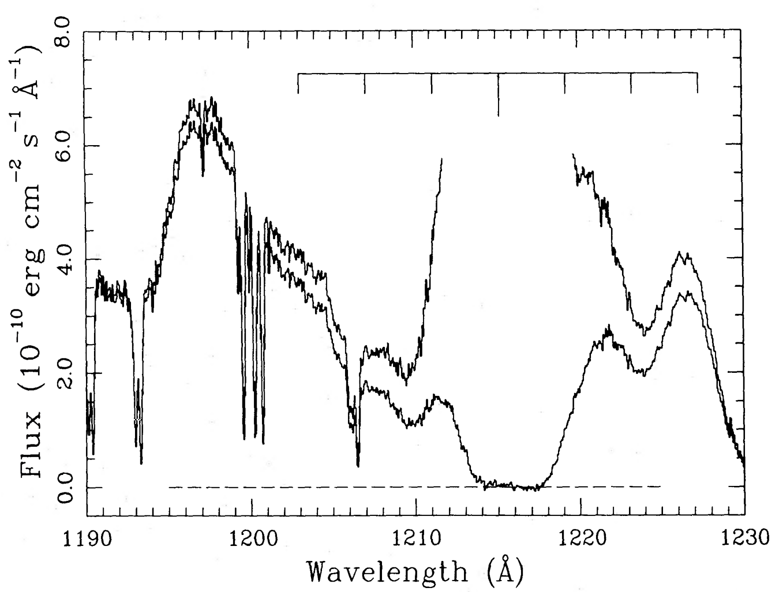

Figure 5. The spectrum of HD 50896 in the region of H Ly-α. The observed data are shown together with the result of correcting for an interstellar H column of 20.7 dex cm^{-2} (upper spectrum). The presence of an intrinsic (stellar) P Cygni profile is demonstrated by these data; a velocity scale (tick-marks every 1000 km s^{-1}) is given above the spectra.

more negative than predicted for He II, apparently supporting an identification of the shifted absorption as arising from H^0 rather than He^+. However, line fluxes in the Pickering series of helium show no evidence for hydrogen in the atmosphere of 50896 (Smith 1973).

Willis found that V_0 for He II $\lambda1640$ is invariably more negative than predicted from the behaviour of other ions (our measurements support this conclusion for 50896). This may be related to the very large optical depths expected for He II Ly-α ($\lambda228$), which should lead to a substantial population in the $n=2$ level. Given this, it is not perhaps surprising that $\lambda1215$, if in fact due to He^+ (as seems likely), is also anomalous; we note that our V_0 for this feature is not very different from that measured for $\lambda1640$. We conclude that it is not possible to discriminate between H^0 and He^+ as the parent ion of the $\lambda1215$ feature in 50896 on the basis of Willis' V_0 – E.P. correlation.

3.2.3 *He II λ1640*

He II Balmer-α, $\lambda1640$, is by far the strongest line in our data, with an equivalent width of ~ -160 Å (Table 4). Although the interpretation of the blueward wing is rendered uncertain by the presence of two N v(?) lines at ~1616 and 1622 A, the red wing is clearly extremely extended; we attribute this extension to the result of electron scattering in the atmosphere. (According to Nussbaumer *et al.* 1982 and Willis *et al.* 1986b N v $\lambda1655.88$ is a contributor to this wing, but a discrete line is not obviously present in our data.) Hillier (1984) has calculated theoretical line profiles for selected helium transitions using a model intended to resemble 50896, including the effects of electron scattering; although his choice of v_∞ is low (1625 km s^{-1}) it may be appropriate for the He II line-forming region.

Fig. 4 compares Hillier's $\lambda1640$ prediction (for a model with $\dot{M}=5\times10^{-5}\,M_\odot\,\mathrm{yr}^{-1}$) with our data. The overall agreement is rather good, particularly in the peak intensity (which Hillier finds to be sensitive to the mass-loss rate adopted), and the red wing. There are some discrepancies in the blue wing, where there is more absorption than predicted by the model; but this does not affect the principal conclusion, that electron scattering is important to line formation in W–R atmospheres.

The N v resonance profile may also show the effects of electron scattering; however, it must be recognized that blending is a serious problem with this doublet.

3.3 THE He II $n\rightarrow3$ SERIES

The $n\rightarrow3$ (Fowler) series of Helium provides a potentially powerful diagnostic of the Wolf–Rayet atmosphere. Apart from $\lambda2254$ ($10\rightarrow3$), which appears to be affected by a blend (probably with a N III line; Willis *et al.* 1986b), the lower members of the series are characterized by FWHM≈1800 km s^{-1} (Table 3). For the highest members that can reliably be separately measured (n=11, 12 and 13), however, there is a strong suggestion of progressive narrowing. Apparently the upper levels are significantly populated only in the inner, accelerating, regions of the wind; these data should therefore provide a useful constraint on detailed wind models.

A systematic velocity shift (observed−laboratory)≈+200 km s^{-1}, appears to be present in the $n\rightarrow3$ series. This may be due to absorption eating into the blue wings, although none of the lines actually exhibit absorption components, and, as Fig. 6 shows, the profiles are generally well approximated by Gaussians. Fig. 6 also shows that electron-scattering wings are not detectable in $7\rightarrow3$; the $6\rightarrow3$ profile does have a feature to the red which may, however, be a blend with another line. He II $5\rightarrow3$ is at the extreme limit of our data, and is affected by gaps between spectral orders; it certainly appears to be asymmetric, and, so far as we can judge, is in good agreement with the profile published by Smith & Kuhi (1981).

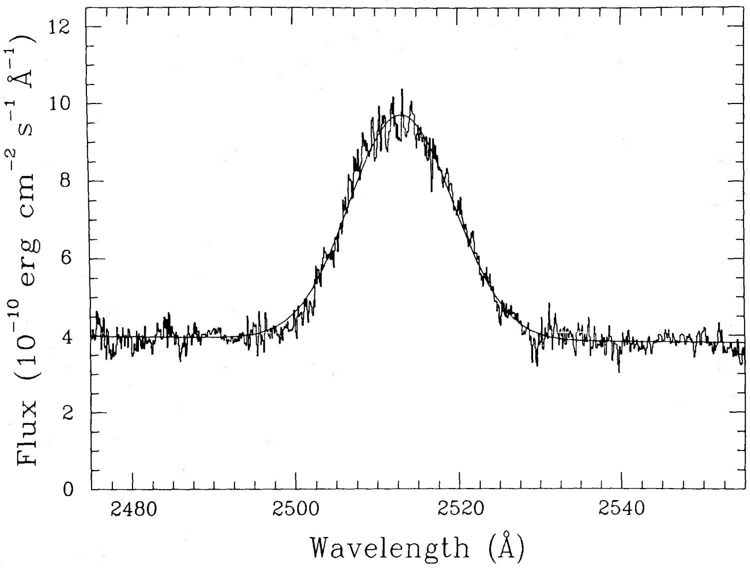

Figure 6. The 7→3 line of He II compared to the Gaussian profile fit given in Table 3.

3.4 2050 Å EDGE

Nussbaumer *et al.* (1982) carried out a Zanstra analysis of the He II emission lines of several WR stars. They pointed out that their model for 50896 predicted an absorption jump (of up to 30 per cent of the continuum level) at 2050 Å, the limit of the $n\rightarrow 3$ series. Unfortunately, this is the noisiest region in our entire data set (S/N≈20). None the less, it is clear (e.g. from Fig. 1) that there is no significant continuum jump ($\Delta I/I<5$ per cent) or change in slope in this region, supporting the conclusion of Schmutz (1982). In the terminology of Nussbaumer *et al.* we conclude that τ_3 is less than 0.1, and on these grounds (at the least) their Zanstra temperature analysis can be questioned. However, our limit on the size of a possible continuum jump is in good agreement with the more detailed models of Schmutz (1984).

Fig. 1 shows that the region ~2000–2100 Å lies significantly above what one might draw in as a continuum level. This is apparently a real effect as it can be seen in the uncalibrated data (i.e. is not an artefact of the flux calibration), as well as being present in the low-resolution spectrophotometry. Presumably this excess is attributable to a blend of unresolved weak emission lines, rather than recombination in the Fowler continuum, given its flat-flux distribution and abrupt disappearance at ~2000 Å.

4 Interstellar-line analysis

4.1 EQUIVALENT WIDTHS

Measurements of interstellar lines in the mean spectra of 50896 are given in Table 5. As might be expected on the basis of signal-to-noise estimates, the weakest lines detected have equivalent widths of order ~5–10 mÅ. A number of lines, spanning a range of ionization potentials, are illustrated in Fig. 7.

The analysis leading to the equivalent-width error estimates given in Table 5 is described in Appendix I. In the present work we assumed that the cross-dispersion order overlap problem has been solved, so that there is no systematic error in the zero level (an assumption supported by the data). We have also assumed that there is no systematic error (in the sense described in Appendix I) in locating the local continuum level; this is amply justified by the very large velocity fields

Table 5. Observations of interstellar lines in the spectrum of HD 50896. Only principal contributors to line blends are listed; wavelengths longer than 2000 Å are air values, otherwise vacuum wavelengths are given. 'HV' means high velocity, and upper limits to equivalent widths are 2σ values.

Ion	λ_{lab}(Å)	λ_{obs}(Å)	f	Source	W_λ(mÅ)	Comments
B II	1362.461	...	0.827	3	<4	
C I	1155.809	...	0.017	1	<30	
	1157.910	...	0.022	1	<30	
	1188.833	1188.77	0.017	2	20±10	Blend with Cl I λ1188.768
	1193.996	1194.02	0.0094	2	9±8	
	1260.736	1260.75	0.0379	1	33±5	
	1276.482	1276.47	0.012	1	7±5	
	1277.245	1277.26	0.156	1	85±7	Blend with C I λ1277.282
	1280.135	1280.17	0.0278	1	28±5	
	1328.833	1328.84	0.0824	1	63±5	
	1560.310	1560.32	0.0810	1	102±9	
	1656.928	1656.94	0.136	1	172±13	Blend with C I** λ1657.008
C I*	1260.927	1261.0 :	0.0126	1	5±3	Broad blend
	1260.996		0.00948	2		
	1261.122		0.0158	1		
	1277.513	1277.54	0.0390	1	24±4	Blend with C I** λ1277.550
	1279.890	1279.91	0.012	2	12±4	
	1329.101	1329.13	0.0824	1	37±4	3 lines
	1560.690	1560.80	0.0808	3	55±6	2 lines
	1656.266	1656.40	0.0566	3	47±7	
	1657.380	1657.49	0.0340	3	44±6	
	1657.907	1658.00	0.0453	3	50±8	
C I**	1261.552	1261.58	0.0284	3	6±4	
	1329.584	1329.59	0.0824	1	10±3	2 lines
	1561.438	1561.45	0.0680	3	10±4	
C II	1334.532	1334.51	0.118	1	556±35	
	"	1334.17				HV
	"	1333.93				HV
C II*	1335.703	1335.69	0.118	1	191±12	2 lines
	"	1335.36				HV
C IV	1548.188	1548.16	0.194	1	447±31	
	"	1547.94				HV
	"	1547.52				HV
	1550.762	1550.75	0.0970	1	337±26	
	"	1550.56				HV
	"	1550.10				HV
N I	1199.549	1199.51	0.133	1	198±14	
	"	1199.21			60±7	HV; blend with Mn II λ1199.388
	1200.223	1200.22	0.0885	1	207±15	Blend with HV N I λ1200.710
	"	1199.90			43±6	HV
	1200.710	1200.69	0.0442	1	174±13	
N II	1083.990	1083.99	0.101	3	198	Shull (1977)
N II*	1084.575	1084.28	0.101	3	0.9	HV; Shull (1977)
N II**	1085.701	1085.70	0.0845	3	12	Shull (1977)
N V	1238.808	1238.84	0.152	1	7±6	
	"	1238.52			44±9	HV
	1242.796	...	0.0757	1	<10	
	"	1242.47			22±7	HV
O I	1302.168	1302.15	0.0486	1	229±15	
	"	1301.81			125±9	HV; blend with P II λ1301.87
	1355.598	...	1.25E-6	1	<4	
O I*	1304.858	...	0.0485	3	<7	
O VI	1037.627	...	0.130	3	<44	Shull (1977)
Na I	5889.950	5890.21	0.665	3	440±30	Smith (1984)
	5895.924	5896.28	0.327	3	295±25	
Mg I	2025.824	2025.79	0.110	1	140:	Overlaps Zn II λ2026.165
	2852.127	2852.09	1.77	1	318±28	
Mg II	1239.925	1239.92	0.00027	7	35±9	
	1240.395	1240.37	0.00013	7	18±8	
	2795.528	2795.52	0.592	1	1091±71	
	"	2794.76				HV
	"	2794.24				HV

Table 5–*continued*

Ion	λ_{lab}(Å)	λ_{obs}(Å)	f	Source	W_λ(mÅ)	Comments
	2802.704	2802.75	0.295	1	885±59	
	"	2802.02				HV
	"	2801.55				HV
Al I	2567.966	2568.73	0.120	3	38±23	
Al II	1670.787	1670.78	1.88	1	335±23	
	"	1670.30				HV
	"	1669.97				HV
Al III	1854.716	1854.78	0.539	1	129±11	
	1862.790	1862.77	0.268	1	94±10	
Si I	1854.520	...	0.152	3	<7	
Si II	1190.416	1190.38	0.29	8	350±26	
	"	1190.13				HV; blend with S III λ1190.206
	1193.289	1193.29	0.58	8	410±30	
	"	1192.99				HV; blend with C I λ1193.031
	1260.421	1260.44	1.12	8	295±10	Blend with Fe II λ1260.542
	"	1260.07				HV
	1304.372	1304.38	0.093	8	174±12	
	"	1304.02			68±7	HV
	1526.708	1526.74	0.12	8	237±17	
	"	1526.35			112±12	HV
	1808.012	1808.04	2.0E-3	8	143±11	
Si II	1194.500	...	0.625	1	<12	
	1264.737	...	0.860	3	<6	
Si III	1206.510	1206.47	1.66	1	398±12	
	"	1206.17				HV
	"	1205.98				HV
Si IV	1393.755	1393.75	0.528	1	186±13	
	"	1393.43				HV
	1402.770	1402.80	0.262	1	167±13	
	"	1402.47				HV
P I	1679.71	...	0.694	3	<5	
P II	1152.81	1152.82	0.236	1	121±27	
	1532.51	1532.51	0.00954	3	7:	
P III	1334.866	1334.84	0.0321	1	13:	
S I	1807.311	1807.39	0.112	3	9±5	
S II	1250.586	1250.57	0.00535	1	134±10	
	1253.812	1253.79	0.0107	1	140±10	
	1259.520	1259.55	0.0159	1	154±11	
	"	1259.22			7±4	HV
S IV	1062.672	1062.70	0.0377	1	45	Shull(1977)
Cl I	1347.24	1347.30	0.112	1	19±4	
Cl II	1071.050	1071.05	0.0159	3	13.9	Shull (1977)
Ar I	1048.218	1048.24	0.230	3	156	Shull (1977)
	1066.660	1066.68	0.0594	3	144	
Ca II	3933.663	3933.84	0.688	3	200±15	L. J. Smith, personal communication
	3968.468	3968.65	0.341	3	120±40	
Ti II	1911.01	...			<4	
	3383.761	3383.93	0.322	3	46	Hobbs (1984)
Ti III	1298.67	...	0.10	9	<4	
V II	2683.078	2683.16	0.0708	3	20±17	
	2739.703	2739.70	0.0398	3	9±9	
V III	1153.190	1153.08	0.10	10	35±26	
	1169.280	1169.37	0.019	10	15±10	
Cr II	2055.59	2055.66	0.109	6	47±9	
	2061.54	2061.57	0.079	6	45±8	
	2065.46	2065.56	0.052	6	36±9	
Mn II	1197.172	1197.15	0.096	1	22±6	
	1201.124	1201.11	0.058	1	10±5	
	2576.105	2576.12	0.288	1	183±29	
	2593.732	2593.73	0.223	1	197±31	
	2605.697	2605.71	0.158	1	143±17	
Fe I	2483.252	...	0.348	3	<33	

Table 5–*continued*

Ion	λ_{lab}(Å)	λ_{obs}(Å)	f	Source	W_λ(mÅ)	Comments
Fe II	1608.456	1608.40	0.0963	5 }	253±21	
	"	1608.08				HV
	2343.495	2343.56	0.150	5 }		
	"	2342.90			749±76	HV
	"	2342.50				Possible HV component
	2373.733	2373.80	0.0419	5	266±37	
	"	2373.14			121±38	HV
	2382.035	2382.03	0.398	5	357±35	
	"	2381.42			221±29	HV
	2585.878	2585.91	0.0846	5 }	495±45	
	"	2586.01				HV
	2599.396	2599.38	0.294	5	385±32	
	"	2598.68			216±25	HV
Co II	1998.55	...			<4	
Ni II	1317.22	1317.22	0.0759	4	25±4	
	1370.13	1370.16	0.0725	4	26±5	
	1454.84	1454.82	0.0256	4	7±4	
	1741.53	1741.54	0.0851	4	24±4	
	1751.91	1751.87	0.0419	4	24±6	
Cu II	1358.773	...	0.46	1	<4	
Zn II	2025.514	2025.51	0.412	1	154±12	
	2062.016	2062.03	0.202	1	104±10	
Ge II	1237.059	1237.05			25±9	See notes
CO	1477.457	...	0.0429	11	<5	

Notes:

Ge II: probably due to another, unidentified, transition (see Morton 1978).

Sources for oscillator strengths are:

1. Morton (1978).
2. Morton (1975).
3. Morton & Smith (1973).
4. K. Butler & P. J. Storey (personal communication).
5. Nussbaumer, Pettini & Storey (1981).
6. Abbott (1978).
7. Hibbert *et al.* (1983).
8. Dufton *et al.* (1983).
9. Wiese & Fuhr (1975).
10. Kurucz (1974).
11. Lassettre & Skerbele (1971).

observed in the stellar spectrum, which ensure that the local continuum level changes slowly and smoothly across the narrow interstellar lines. Local continua were approximated by low-order Chebyshev polynomials in order both to rectify the data and to estimate S/N ratios.

Fig. 8 compares equivalent widths measured in our *IUE* data with results from *Copernicus* scans reported by Shull (1977). The good agreement provides further confirmation that our zero level is satisfactory.

4.2 LINE PROFILE ANALYSIS

Most of the interstellar absorption features are blends of several velocity components or closely spaced lines; thus profile fitting is the only satisfactory method for determining column densities. We therefore calculated theoretical line profiles, adjusting the free parameters by trial and error until we achieved what we judged to be a 'best fit' to *all* the lines arising from a given lower level. In this way we could assess the sensitivity of the fits to the adjustable parameters, give low weight to lines with suspect atomic data, and obtain (subjective) error estimates.

The code we used to carry out the profile calculations is one originally due to Davenhall (1977), ported to STARLINK by one of us (APP), and modified by C. K. Thomas and D. E. Maslen for

1986MNRAS.222..809H

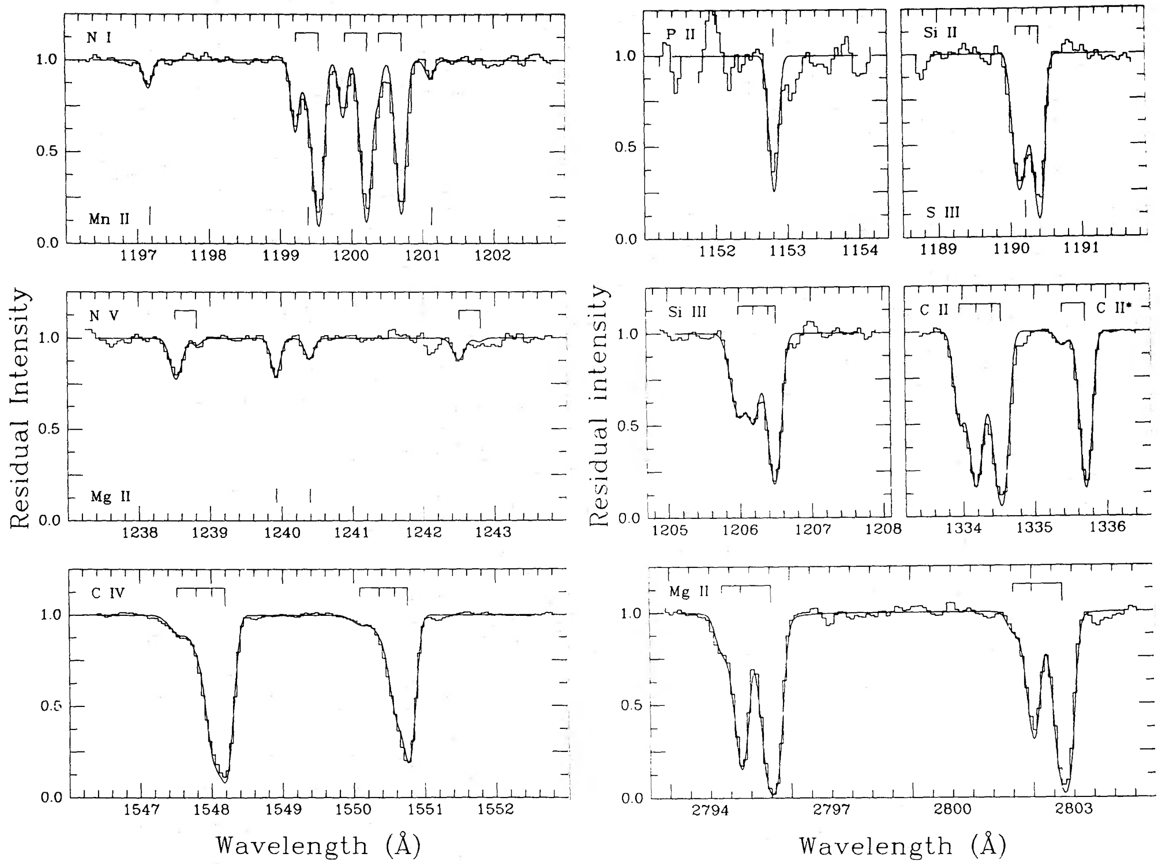

Figure 7. Comparison of observed and modelled line profiles for selected features. Different lines are marked by long vertical ticks, and multiple-velocity components by offset shorter ticks.

interactive use. It incorporates the customary assumptions and physics, as described by Strömgren (1948). After completing this profile analysis we used an independent program (written by J. R. Giddings) to re-analyse several ions and complex blends (like the N I $\lambda1200$ feature). This program solves for column density by least squares (with velocities and velocity

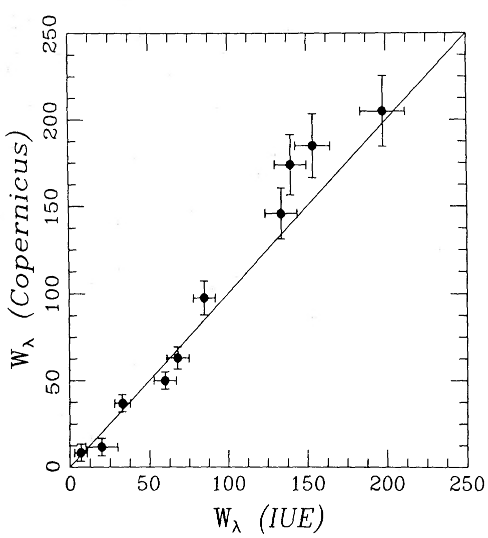

Figure 8. A comparison of equivalent widths (in mÅ) measured from *Copernicus* data (Shull 1977) and *IUE* spectra (this paper). An error of 10 per cent (or 5 mÅ, if larger) has been assumed for the *Copernicus* data, based on results from repeat scans.

dispersions fixed). The results fully confirm those of the complete analysis, including our error estimates which, within the framework of the adopted cloud model, we judge to be pessimistic.

4.2.1 Instrumental resolution

Most of the lines are, at best, only marginally resolved. An important parameter in the profile fitting is, therefore, the instrumental point-spread function (psf), which we assumed to be Gaussian in form. Although we could have adopted a canonical value for the instrumental FWHM, as previous workers have done, we considered this a somewhat precarious step to take for several reasons. First, and most importantly, it is clear that the psf along the direction of dispersion is simply not accurately known for *IUE* in high-resolution mode. Secondly, the low-resolution psf is known to vary as a complex function of the physical status of the spacecraft (Cassatella, Barbero & Benvenuti 1985), and high-resolution spectra might be expected to be similarly affected; the FWHM appropriate to our mean spectrum (or, indeed, to any single spectrum contributing to it) is therefore uncertain. Finally, we may suspect that in combining many spectra slight wavelength misalignments may result in a broadening of the effective psf (although our data-reduction procedures should minimize this problem, and comparison of the individual spectra with the mean spectrum does indeed show that any loss of resolution thus incurred is, in fact, undetectable).

To overcome the uncertainty in the psf we constructed empirical curves of growth for all the relatively blend-free lines in the low-velocity system. We then compared these with theoretical single-cloud models, assuming a Gaussian line-of-sight velocity distribution with an rms velocity dispersion of $b/\sqrt{2}$ for the absorbers:

$$\Psi(v)=\frac{1}{\pi^{1/2}b}\exp\left[-\frac{(v-v_0)^2}{b^2}\right].$$

Contributions to b come from the thermal velocities of the ions and a 'turbulent velocity' parameter (which usually dominates in practice):

$$b=\left(\frac{2kT}{m}+2v_t^2\right)^{1/2}.$$

We found that all lines in the *IUE* range due to neutrals and first ions could be represented by a theoretical curve of growth with a velocity dispersion parameter b of 10.5 km s^{-1} (see Fig. 9). This value is in good agreement with that found by Shull (1977) for most species in his *Copernicus* survey. Unacceptably bad fits result if b is outside the range 9.0–12.5 km s^{-1}.

Adopting $b=10.5$ km s^{-1}, and provisional estimates of column densities obtained from the curve of growth, we calculated line profiles for a range of instrumental FWHMs. Good fits to the observed profiles were obtained by adopting FWHM=30 km s^{-1} in both cameras at all wavelengths (i.e. resolving power $R=10^4$; $b_{\rm inst}=18$ km s^{-1}). This is consistent with the results given by Boggess *et al.* (1978) in their description of the performance of the *IUE* scientific instrument.

4.2.2 Results

We find evidence for four velocity systems: low-velocity (LV) gas, and blueshifted absorptions at ≈ -30, -75, and -130 km s^{-1}. The low-velocity system includes contributions from both neutral and H II region species. The adopted fit parameters for each component are summarized in Table

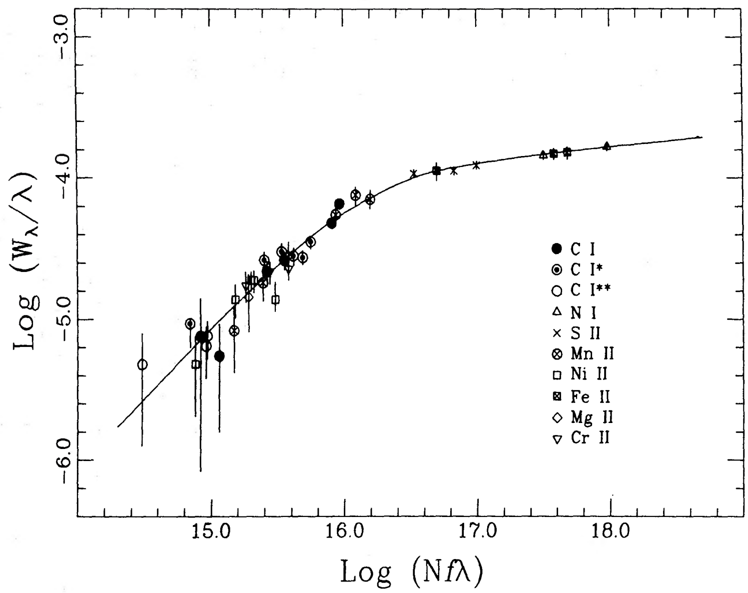

Figure 9. The empirical curve of growth for ions formed in the low-velocity H I system having more than one line reliably measured. A theoretical CoG for a single cloud model having $b=10.5\,\mathrm{km\,s^{-1}}$ is shown for comparison.

6, and some profile fits are illustrated in Fig. 7. Within the accuracy of our data, there are *no* systematic trends of either central velocity or b values with ionization potential.

The b values used for high-velocity features are generally quite uncertain, and are based on a combination of profile shapes and (for doublets) equivalent-width ratios. For example, the very small b used for the $-75\,\mathrm{km\,s^{-1}}$ component seen in Si IV arises because the doublet ratio is materially larger than 0.5. For other lines we generally started (arbitrarily) with $b=10$ or $20\,\mathrm{km\,s^{-1}}$ and then 'tweaked' to optimize the profile fits. We therefore caution that these b values should not be interpreted too literally.

Column density error estimates in Table 6 are based on the extreme ranges of (b, N) values giving acceptable profile fits to all lines of a given species, or to a range of $\pm 1.5\,\mathrm{km\,s^{-1}}$ in b; in every case, we give the larger of the resulting error estimates. Upper limits for lines not explicitly listed can be estimated by assuming $W_\lambda < 10\,\mathrm{m\AA}$ (SWP) or $20\,\mathrm{m\AA}$ (LWR).

As noted previously, experiments with a least-squares modelling code support the conservative nature of the errors we quote on column densities (which include a contribution from the uncertainties in b), with two caveats. First, if the adopted cloud model is wrong then the errors are, of course, inappropriate. [In the most plausible case, where additional unresolved components are present in a given velocity system, then our derived column densities can be regarded as lower limits (Nachmann & Hobbs 1973).] Secondly, we have made no explicit allowance for uncertainties in the adopted atomic data (although our error estimates should include a contribution from *random* errors in the f values). As a specific example we cite Si II, for which two sets of recent f values are available: Dufton *et al.* (1983), and Shull, Snow & York (1981). Neither data set gave entirely satisfactory fits (in fact, we found the Si II spectrum to be the most resistant to a consistent parameterization, reflected in the errors given in Table 6), but the Dufton *et al.* values gave the better overall agreement. However, using their f value for λ1808, which is relatively weak (and therefore the most useful line for estimating the column density), gave hopelessly poor line fits for the adopted parameters. Adequate fits could only be obtained by assuming an oscillator strength of $(0.5–1.5)\times10^{-2}$, which is more nearly consistent with Shull *et al.*'s value. Had we relied more heavily on the λ1808 line and Dufton's *et al.*'s oscillator strength, we could therefore have arrived at a Si^+ column density some five times greater than that actually

Table 6. Model parameters adopted from profile fits to interstellar lines. Data for optical lines are taken from the sources cited in Table 5. (Shull 1977 quotes upper limits to high-velocity Ar I equivalent widths, but gives an actual value for the column density, which is reproduced here.)

Ion	Velocity	b	log N
B II	LV	10.5	<11.5
C I	LV	10.5	13.87 ± 0.10
C I*	LV	10.5	13.65 ± 0.08
C I**	LV	10.5	$12.93^{+0.12}_{-0.17}$
C II	LV	10.5	$15.48^{+0.52}_{-0.18}$
	-27	10	13.70 ± 0.21
	-81	21	14.41 ± 0.07
	-134	10	13.84 ± 0.07
C II*	LV	10.5	14.95 ± 0.13
	-72	19	12.95 ± 0.13
	(-130)		<12.3
C IV	LV	11.5	14.3 ± 0.3
	-35	20	14.00 ± 0.16
	-77	20	13.08 ± 0.09
	-130	30	$12.95^{+0.20}_{-0.10}$
N I	LV	10.5	$15.5^{+0.8}_{-0.3}$
	-78	6	13.82 ± 0.12
N II	LV		$15.8^{+0.9}_{-0.6}$
	-78		14.39 ± 0.10
N II*	-81		11.94 ± 0.10
N II**	LV		13.12 ± 0.03
N V	LV	10.5	≤12.5
	-72	20	13.40 ± 0.08
O I	LV	10.5	16.6 ± 0.6
	-74	14	14.50 ± 0.07
O I*	LV		<13.0
O VI	LV		<13.55
Na I	LV		12.54
	-18.0		11.90
Mg I	LV	10.5	13.30 ± 0.07
Mg II	LV	10.5	$16.08^{+0.10}_{-0.13}$
	-80	15	13.43 ± 0.10
	-130	15	12.36 ± 0.10
Al I	LV	10.5	$12.85^{+0.24}_{-0.43}$
Al II	LV	12	13.15 ± 0.06
	-80	22	12.50 ± 0.06
	-140	25	11.73 ± 0.06
Al III	LV	10.5	13.20 ± 0.07
Si I	LV		<12.2
Si II	LV	10.5	15.00 ± 0.30
	-30	5	12.80 ± 0.30
	-80	10	13.85 ± 0.20
	-130	20	≤12.5
Si II*	LV		<11.7
Si III	LV	10.5	13.40:
	-25	15	12.70:
	-77	20	12.75 ± 0.02
	-130	30	12.85 ± 0.03
Si IV	LV	10.5	13.74 ± 0.20
	-30	>3	12.48 ± 0.12
	-70	2	$13.08^{+0.50}_{-0.27}$
	-133	20	≤12.0
P I	LV		<11.5
P II	LV	10.5	$14.21^{+0.44}_{-0.35}$
P III	LV	10.5	13.43:
S I	LV	10.5	$12.46^{+0.20}_{-0.36}$
S II	LV	10.5	15.70 ± 0.16
	-77	15	13.51 ± 0.21
S III	LV	10.5	14.65 ± 0.30
	-30	10	≤14.0
S IV	LV		14.20
Cl I	LV	10.5	13.06 ± 0.10
Cl II	LV		13.94 ± 0.10
Ar I	LV		$15.25^{+0.30}_{-0.20}$
	-75:		12.70 ± 0.10
Ca II	LV		12.46
Ti II	LV		12.18
Ti III	LV		<12.5
V II	LV	10.5	$12.67^{+0.28}_{-0.84}$
V III	LV	10.5	$13.73^{+0.29}_{-0.58}$
Cr II	LV	10.5	13.20 ± 0.08
Mn II	LV	10.5	13.33 ± 0.14
Fe I	LV		<12.3
Fe II	LV	10.5	$14.70^{+0.33}_{-0.29}$
	-77	9	13.76 ± 0.19
Ni II	LV	10.5	13.31 ± 0.10
Cu II	LV		<11.7
Zn II	LV	10.5	13.26 ± 0.06
CO	LV		<12.8

adopted★. Other species where similar problems perhaps exist include Cr^+ and V^{2+}, since large systematic errors may be present in the sources of f values we adopted.

4.2.3 *Other components?*

Shull (1977) reported a further component at $-96\,\mathrm{km\,s^{-1}}$, seen in both N II (unobservable with

★ After completing this paper we learnt that Dufton now believes the Shull *et al.* oscillator strength for $\lambda1808$ to be the more reliable.

IUE) and Si II. Although we are hampered by inadequate resolution, we see no sign of the $-96\,\mathrm{km\,s^{-1}}$ feature in our data. In particular, our b value for blueshifted Si II is not so large as to suggest that we have inadvertently modelled two clouds, well separated in velocity space, as a single feature. Uncertainties in the adopted oscillator strengths make some of our Si II profile fits rather poor, but we can none the less conclude that the column density of Si^+ at $-96\,\mathrm{km\,s^{-1}}$ is $\lesssim 13.0\,\mathrm{dex\,cm^{-2}}$. Shull did not give a column density for Si^+ at $-96\,\mathrm{km\,s^{-1}}$, but did report one for N^+. Assuming the two ions to be in the ratio of their cosmic elemental abundances would suggest $N(Si^+)=13.2\,\mathrm{dex\,cm^{-2}}$, which is not in serious discord with our upper limit.

Possible additional absorption systems are hinted at in our data at $+67\,\mathrm{km\,s^{-1}}$ (Si III, C II) and $+83\,\mathrm{km\,s^{-1}}$ (C IV; see Fig. 7). Nothing is seen in Si IV at these velocities. We do not consider further any of the features noted in this sub-section.

5 Hydrogen column

Before proceeding to a discussion of element depletions, we need to establish the hydrogen column density along the line-of-sight. We can do this by three means (only the last of which is useful for decomposing the total column into the various velocity systems observed).

5.1 REDDENING

There is a reasonable correlation between hydrogen column density and extinction along most sightlines (Savage *et al.* 1977; Bohlin, Savage & Drake 1978). However, the interstellar reddening in the line-of-sight to HD 50896 is uncertain. In the absence of accurately known intrinsic optical colours (Massey 1984) the most straightforward method for estimating $E(B-V)$ is to deredden the ultraviolet fluxes until the 2200 Å feature is nulled; unfortunately, this approach also has its dangers in that the extinction curve itself may not be 'normal'. In particular, Wolf–Rayets may be subject to peculiar circumstellar extinction, which could vitiate results obtained using this method (e.g. Garmany, Massey & Conti 1984). Moreover, the interstellar extinction curve is modified if grains are sputtered (see Seab & Shull 1983), and the 2200 Å feature may be strengthened per unit colour excess. This might be considered a very real possibility in this sightline in the light of the results to be given in Section 6. However, the bulk of the interstellar material toward 50896 ($\gtrsim 99$ per cent) is at low velocity. Moreover, S2/68 UV spectrophotometry of the field stars described in Section 8 is, in each case, consistent with the optically determined spectral types and reddenings. We conclude that a standard extinction curve is unlikely to give results seriously in error for 50896, and adopt the analytical representation given by Seaton (1979).

Most previous attempts at nulling the 2200 Å feature have found essentially zero extinction (e.g. Nussbaumer *et al.* 1982 and references therein). However, we think that these attempts have been frustrated by what we can, with hindsight, identify as a lack of resolution. Our flux-calibrated spectrum is shown in Fig. 1; it can be seen at once that the reddening is low, in agreement with previous reports. However, considerable structure is present in the stellar spectrum around 2200 Å, including the raised 'continuum' noted in Section 3.3. This structure, only marginally resolved in previous flux-calibrated spectra, has, we believe, led to underestimates of the strength of the 2200 Å feature. In our data the interstellar band is quite clearly present (most obviously in a log–log plot), and from its strength we estimate $E(B-V)=0.10\pm0.04$. This value is in excellent agreement with the estimates made by Nussbaumer *et al.*, from line strengths of He II [$E(B-V)=0.08$], and by Smith (1968) [also $E(B-V)=0.08$], from optical colours.

At such low reddenings the correlation between hydrogen column density and $E(B-V)$ is rather poor. None the less, using the data summarized by Savage & Mathis (1979) we can use the observed extinction to estimate $N(H^0)=20.7$, $N(H^0+H_2)=20.8\,\mathrm{dex\,cm^{-2}}$ (both $\pm\sim0.3$).

5.2 HYDROGEN Ly-α

On the (safe) assumption that the interstellar H Ly-α profile is fully damped, and neglecting the velocity dispersion between different components, we can estimate the interstellar neutral hydrogen column by dividing the observed profile by a theoretical one (in the manner of Bohlin *et al.* 1978) until the underlying stellar spectrum is restored.

As noted in Section 3.2.2, the underlying stellar spectrum undoubtedly contains a strong P Cygni feature which is most probably attributable to He II λ1215.2. The usual procedure of 'flattening' the spectrum is therefore inappropriate in the present case. However, we can obtain at least an upper limit to $N(H^0)$ by requiring that the wings of λ1215 (assumed to be due to He II Balmer-β) indicate a stellar feature no stronger than λ1640 (He II Balmer-α). Plausibility of the reconstructed stellar spectrum provides a reasonably safe lower limit (bearing in mind that the stellar profile varies exponentially with the adopted interstellar H^0 column). In this way we find $20.85 \geqslant \log[N(H^0)/cm^{-2}] \geqslant 20.6$.

The value of $N(H^0)=20.54$ dex cm^{-2} determined both from *Copernicus* data by Bohlin *et al.* (1978) and from *IUE* data by Shull & Van Steenberg (1985) is smaller than our lower limit. We think that this is because they sought to reconstruct a flat stellar spectrum, and neglected the importance of He II Balmer-β emission. However, the molecular hydrogen column determined in the same way is unaffected by this problem, and so we can accept published values: $N(H_2)=19.3$ (Savage *et al.* 1977) or 19.5 (Shull 1977) dex cm^{-2}, and $N(HD)=14.2$ dex cm^{-2} (Shull 1977).

5.3 SCALING FROM GAS-PHASE ELEMENTS

It is generally found that sulphur and zinc are undepleted in neutral clouds in the diffuse interstellar medium (e.g. Spitzer & Jenkins 1975; York & Jura 1982). On the assumption of zero depletion we can therefore derive hydrogen column densities in each of the velocity systems in which we observe the dominant ions of these elements. For velocity systems where the dominant species are not observed, or for elements where depletion from the gas phase is likely (Section 6), we can set lower limits. Using Snow's (1980) compilation of solar abundances, this method gives the following results: for the low-velocity gas $\log N(H^0)=20.7$ (from S, Zn), $\log N(H^+)=19.6$ (from S, supported by N and P); for the -30 km s^{-1} component, $\log N(H) \lesssim 19$ (from S), >17.6 (from C, Si); for the -75 km s^{-1} component, $\log N(H)=18.3$ (from S); and for the -130 km s^{-1} component $\log N(H) \lesssim 18.6$ (from S), $\geqslant 17.3$ (from S, C, and Al).

These numbers are subject to at least two sources of error. First, there is some evidence that S (and possibly even Zn) may be slightly depleted in some sightlines, by an amount which probably correlates with mean line-of-sight hydrogen space density (e.g. Tarafdar, Prasad & Huntress 1983; Harris, Gry & Bromage 1984). This is unlikely to be important at our level of accuracy, particularly since the 50896 sightline has a conspicuously low value for $\langle n(H) \rangle$ (Section 5.4). (Table 7 reveals an apparently real differential depletion of S with respect to Zn in our data, but in fact this difference can be readily accommodated by the uncertainties in the appropriate solar values. For example, using the results compiled by Cowie & Songaila 1986, instead of Snow's values, would revise $\Delta\delta$ from 0.36 ± 0.17 to a negligible 0.16 ± 0.17.) Secondly, we will argue in Section 9 that the -30 km s^{-1} component arises in the nebula S308. If this is correct then the assumption of cosmic abundances to estimate the hydrogen column for this system will be in error, since the nebular material will consist of swept-up interstellar matter mixed with gas from the stellar wind of 50896, and the stellar wind almost certainly contains the products of nuclear processing. Simple calculations indicate, however, that the effects of mixing are unlikely to influence the derived H columns seriously; plausible assumptions actually lead to the quoted lower limit being raised somewhat.

Table 7. Depletions. Errors of 0.3 dex in the observed columns have (arbitrarily) been assigned to the total columns of Na and Ca (for which the ionization fractions of dominant ions have been calculated; Section 6), and to Ti (from Hobbs 1984). Errors given for depletions do *not* include any contributions from the uncertainties in the hydrogen column (although the error bars in Fig. 11 do allow for the errors in this quantity quoted in the table). The adopted solar abundances are those given by Snow (1980).

a. Depletions in LV H I system.

Spectra		$\odot$	Column	Depletion
H	I	12.0	20.70	0.0 ± 0.15
B	II	2.30	<11.5	$<+0.5$
C	I+II	8.57	15.61	$-1.66^{+0.39}_{-0.14}$
N	I	8.06	15.50	$-1.26^{+0.80}_{-0.30}$
O	I	8.83	16.60	-0.93 ± 0.60
Na	I(+II)	6.24	14.73	-0.21 ± 0.30
Mg	I+II	7.54	16.08	$-0.16^{+0.10}_{-0.13}$
Al	I+II	6.40	13.33	$-1.77^{+0.09}_{-0.15}$
Si	II	7.55	15.00	-1.25 ± 0.30
P	II	5.50	14.21	$+0.01^{+0.44}_{-0.35}$
S	I+II	7.21	15.70	-0.21 ± 0.16
Cl	I+II	5.3:	13.99	-0.01 ± 0.09
Ar	I	6.65:	15.25	$-0.10^{+0.30}_{-0.20}$
Ca	II(+III)	6.33	13.27	-1.76 ± 0.30
Ti	II	4.74	12.18	-1.26 ± 0.30
V	II	4.10	12.67	$-0.13^{+0.28}_{-0.84}$
Cr	II	5.70	13.20	-1.20 ± 0.08
Mn	II	5.42	13.33	-0.79 ± 0.14
Fe	II	7.40	14.70	$-1.40^{+0.33}_{-0.29}$
Ni	II	6.28	13.31	-1.67 ± 0.10
Cu	II	4.45	<11.7	<-1.45
Zn	II	4.42	13.26	$+0.14 \pm 0.06$

b. Depletions in -75 km/s component

Spectra		$\odot$	Column	Depletion
H	I+II	12.0	18.30	0.0 ± 0.20
C	II+IV	8.57	14.44	-0.43 ± 0.06
N	I+II+V	8.06	14.53	$+0.17 \pm 0.08$
O	I	8.83	14.50	$\geq -0.63 \pm 0.07$
Mg	II	7.54	13.43	$\geq -0.41 \pm 0.10$
Al	II	6.40	12.50	-0.20 ± 0.06
Si	II+III+IV	7.55	13.95	$+0.10 \pm 0.17$
S	II	7.21	13.51	$+0.00 \pm 0.21$
Ar	I	6.65:	12.70	$\geq -0.25 \pm 0.10$
Fe	II	7.40	13.76	$+0.06 \pm 0.19$

5.4 DISTANCE TO 50896, AND ADOPTED H COLUMNS

The preceding discussion has yielded several consistent estimates of hydrogen column densities towards 50896; we adopt

$\log N(\mathrm{H}^0) = 20.70 \pm 0.15$;
$\log N(\mathrm{H}_2) = 19.40 \pm 0.20$;
$\log N(\mathrm{HD}) = 14.2 \pm 0.4$; and
$\log N(\mathrm{H}^+) = 19.60 \pm 0.20$ in the low-velocity gas;
$\log N(\mathrm{H}) \approx 18.3 \pm 0.7$: in the $-30\,\mathrm{km\,s^{-1}}$ component;

$\log N(H^0+H^+)=18.30\pm0.20$ in the $-75\,\mathrm{km\,s^{-1}}$ component; and
$\log N(H^0+H^+)\approx17.6^{+1.0}_{-0.3}$ in the $-130\,\mathrm{km\,s^{-1}}$ component.

The distance to HD 50896 is usually quoted as 1.5 kpc on the basis of the apparent magnitude and Smith's (1973) absolute-magnitude calibration. However, since Smith's work it has become clear that there is a considerable spread in intrinsic luminosity at all sub-types (Garmany, Conti & Chiosi 1982); the distance is therefore uncertain. Adopting the calibration between spectral type and absolute magnitude given by Lundström & Stenholm (1984), together with the (Smith) v magnitude that they quote for 50896 and the reddening derived in Section 5.2, gives $D=1.8$ kpc. On the other hand, if 50896 is a member of the loose cluster Cr 121 then it may be as close as 0.9 kpc (Lundström & Stenholm 1984). Since the results of Sections 8 and 9 (in particular, Section 9.1) tend to favour the more distant value, we tentatively adopt $D=2$ kpc. The resulting mean line-of-sight hydrogen space density ($\mathrm{cm^{-3}}$) is $\log\langle n(\mathrm{H})\rangle\approx(-1.1\pm0.2{:})$.

6 Element depletions

We define the depletion of an element X as

$$\delta_X=\log[N(X)/N(\mathrm{H})]-\log[N(X)/N(\mathrm{H})]_\odot,$$

where we adopt the solar abundances given by Snow (1980). The usual presumption is that material missing from the gas phase is locked in the grains responsible for interstellar extinction. In this section we examine depletions in each velocity system, so far as is possible.

6.1 LOW-VELOCITY COMPONENT

6.1.1 H^0 gas

The high b value found for the low-velocity component evidently reflects the bulk motion of several unresolved clouds. Shull (1977) used *Copernicus* data to investigate this component in some detail. His results largely complement those presented here; his data had better resolution, but poorer signal-to-noise, and mainly covered different lines. Fig. 10 compares our column

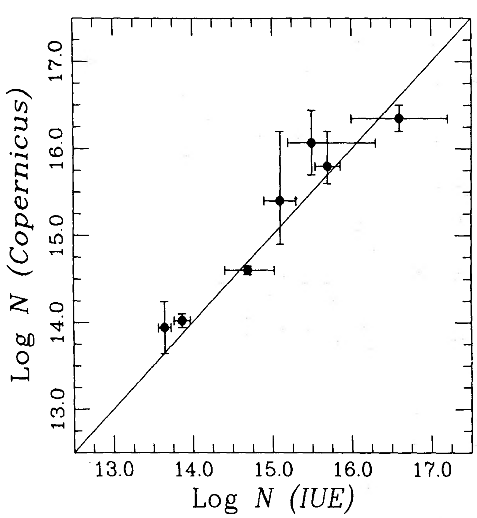

Figure 10. Comparison of column densities (in units of $\mathrm{cm^{-2}}$) for low-velocity H I system species derived from *Copernicus* (Shull 1977) and *IUE* data.

densities with Shull's; even at high values of N, where saturation effects are most likely to be important, agreement is good.

Shull identified a minimum of three cloud components in the low-velocity system: a molecular hydrogen cloud containing ~20 per cent of the neutral gas; and (on the basis of small asymmetries in Ar I and Fe II lines shortwards of the *IUE* wavelength limits) two further neutral components with a velocity separation of $\sim 10\,\mathrm{km\,s^{-1}}$. Neither we nor Shull were able to measure columns separately for the two principal components; therefore our columns, parameterized by a single b value which largely reflects the bulk relative velocities of the component clouds, should be regarded as lower limits to the true values, as should (numerically) our depletions. However, for many ions we have detected weak lines which are at worst only barely saturated, and we think that our modelled columns therefore probably represent the true columns reasonably well (see, too, Jenkins 1986). Unfortunately, the elements for which our estimated columns are most likely to be wrong (probably in the sense of being too small), and our errors optimistic, are the important CNO group, for which no weak lines of dominant ions are available.

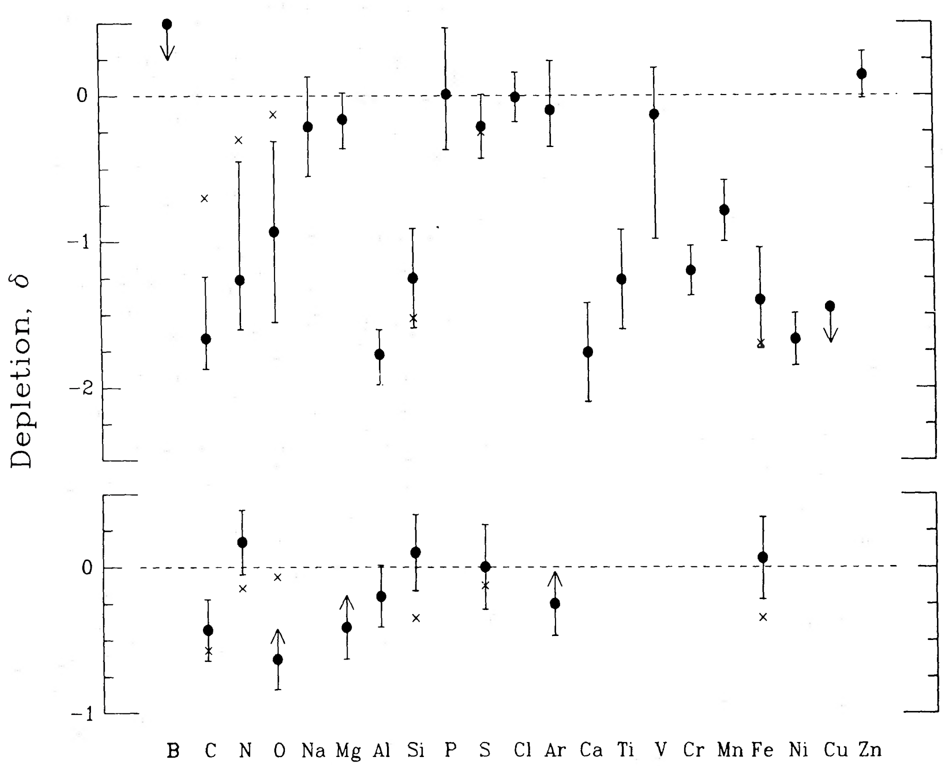

Figure 11. Depletions found for the low-velocity H I system (upper section) and for the $-75\,\mathrm{km\,s^{-1}}$ system. Crosses show the 'standard' depletion pattern adopted by Seab & Shull (1983; upper section) and the abundances they predict following processing by an $80\,\mathrm{km\,s^{-1}}$ shock.

Depletions derived for the low-velocity H I gas are summarized in Table 7(a) and Fig. 11. For most elements observations are available for all ionization stages likely to be important in the H I gas. This is not true, however, for Ca and Na; for these two elements we calculated the likely contributions of unobserved dominant species (Na^+, Ca^{2+}) by assuming that equilibrium ionization balance is maintained between electron-collision recombination and valence-shell photoionization by the interstellar radiation field. To eliminate the need to know explicitly an appropriate mean electron density we appeal to the observed ionization balance for Mg (which has ionization potentials not too dissimilar to those in which we are interested, and for which column densities are quite precisely known); then

$$\frac{n(X^{i+1})}{n(X^i)}=\frac{n(\mathrm{Mg}^+)}{n(\mathrm{Mg}^0)}\times\frac{\Gamma(X^{i+1})}{\Gamma(\mathrm{Mg}^0)}\times\frac{\alpha(\mathrm{Mg}^0)}{\alpha(X^i)}\times\frac{n_e}{n_e},$$

where $\Gamma(X)$ is the photoionization rate of element X, $\alpha(X)$ is the corresponding recombination coefficient, and X^i is Na^0 or Ca^+. We adopted the atomic data summarized by Phillips, Pettini & Gondhalekar (1984a), and the radiation field derived by Gondhalekar, Phillips & Wilson (1980), to obtain the requisite ionization corrections.

These data also lead to an estimate of $n_e \sim -1.2\,\mathrm{dex\,cm^{-3}}$ in the low-velocity neutral gas. Although this value is sensitive to the adopted radiation field, the required ionization corrections are more robust since they depend not on the absolute value of the radiation field (nor on n_e) but only on the ratio of the Γs.

6.1.2 H^+ gas

Smith *et al.* (1980) first drew attention to the strength of the C IV and Si IV features in the spectrum of 50896. We also detect strong lines of Al III and Si III, and find evidence for N V, P III, and S III, while Shull (1977) gives a measurement for S IV, and an upper limit for O VI. HD 50896 thus has probably the richest UV H II region absorption spectrum yet reported in the literature.

In modelling the lines from high ions, we found that the same b value for H I region lines, $10.5\,\mathrm{km\,s^{-1}}$, again gave good profile fits; presumably this is no more than coincidence. Fig. 7 illustrates the results of profile fitting for selected species. Several lines show an extended blue wing, which we have interpreted as evidence for a component at $\sim -30\,\mathrm{km\,s^{-1}}$; this feature is discussed in Section 6.2.

From the observed column density ratios it seems probable that the second and third ions of silicon and sulphur are the dominant species for these elements. Assuming S to be undepleted, as it is in the neutral gas, we have $\delta_{\mathrm{Si}}=-1.22\pm0.34$, which is almost exactly the same value as found in the LV H I system. However, for aluminium we find $\delta \geqslant -0.8$, a dex or more greater than in the neutral gas. We take this as evidence for partial sputtering of dust grains; further discussion is given below (Section 6.5).

The V^{2+} column reported in Table 6 implies an overabundance with respect to solar values of 2 dex (or a corresponding depletion of S). It is likely to be spurious unless (as is quite possible) the adopted oscillator strength is seriously in error.

6.2 THE $-30\,\mathrm{km\,s^{-1}}$ COMPONENT

As noted above, in order to obtain satisfactory fits to a number of line profiles we were forced to adopt a component at $\sim -30\,\mathrm{km\,s^{-1}}$. [Rather poorer, but still acceptable fits could also be achieved for some ions by using very large b values for the low-velocity component (20–$30\,\mathrm{km\,s^{-1}}$) and slightly blueshifted central positions, but we consider this interpretation less plausible; a continuous velocity distribution bluewards from rest is another possibility, but we have not modelled the data on the basis of this interpretation.] Clearly, substantially better resolution is required to establish the nature of this feature, but our confidence in its reality is boosted by examination of Shull's (1977) *Copernicus* scan of Si III λ1206 which, although of quite poor signal-to-noise, confirms the anomalous width of this line as seen in our data. L. J. Smith's (1984, personal communication) high-quality optical observations of Na I ($R \approx 4\times10^4$) also show a significantly blueshifted feature, but with a velocity offset of only $\sim 18\,\mathrm{km\,s^{-1}}$, suggesting that either a different cloud is recorded in her data, or that a velocity gradient exists across the line-forming region.

Any quantitative discussion of the $-30\,\mathrm{km\,s^{-1}}$ system is severely hampered by our limited resolution. It is apparently present in a wide range of ions (C^+ to C^{3+}), but is not detected in strong lines of Mg I, Mg II, or Fe II. Although this appears to suggest that it is produced in a region of moderately high ionization, if a velocity gradient does exist such that H I region ions (like Na I) are at lower velocities then we would not necessarily expect to detect them at our resolution.

Velocity dispersions are poorly determined; b values of 10–20 $\mathrm{km\,s^{-1}}$ give reasonable fits. The column density estimates given in Table 6 are insensitive to the exact value of b, since the lines suffer little saturation, and from the observed abundances we have inferred a hydrogen column density of at least $\log N(\mathrm{H})=17.6$ (Section 5.3). We can say nothing definite about possible depletions, however, since although the observed columns of C, Na and Si all yield about the same value for $N(\mathrm{H})$ (hinting at complete grain destruction), important species such as C^{2+} are unobserved. The upper limit to the hydrogen column derived from the absence of detectable S lines is not low enough to be of interest in this context.

6.3 THE $-75\,\mathrm{km\,s^{-1}}$ FEATURE

The $-75\,\mathrm{km\,s^{-1}}$ component is the second strongest in many lines, containing ~½ per cent of the total gas in the line-of-sight. It is seen in a very wide range of ions, from N^0 to N^{4+}; many have sufficiently well-resolved lines that it is possible to back up the profile fits with simple curve-of-growth calculations. Velocity dispersions are rather large, and again poorly determined; $b\approx 10$–$20\,\mathrm{km\,s^{-1}}$. However, because of these large b values, the lines are essentially unsaturated, and so column densities are reasonably accurately known.

Depletions are summarized in Table 7 and Fig. 11. Corrections for unobserved species are difficult to estimate, since simple equilibrium models will not reproduce the observed ionization ratios; given the absence of detectable Al III, and the relatively small Si^{2+} column, we have assumed for the purposes of Table 7 that ionization of species with IP>16 eV is unimportant. In any event, it is clear that there is no substantial depletion of any element in the $-75\,\mathrm{km\,s^{-1}}$ component, implying essentially complete grain destruction in this velocity system. (Carbon may be slightly depleted, although C^{2+} is unobservable.) We discuss this result further in Section 6.5.

6.4 THE $-130\,\mathrm{km\,s^{-1}}$ COMPONENT

The strongest lines show a fourth component at $\approx -130\,\mathrm{km\,s^{-1}}$. Both H I and H II region species are seen. The lines are all weak, and on the linear part of the curve-of-growth.

The column densities for C, Al and Si, summed over observed ions, are in the same ratios as cosmic values; for Al and Si, at least, the dominant ions are probably recorded. We take this to indicate that grain destruction has probably taken place in this absorption system, although the lower limits to possible depletions implied by the absence of detectable S are too weak to confirm this. If grain destruction is total then $N(\mathrm{H})=17.3\,\mathrm{dex\,cm^{-2}}$ (Section 5.4).

6.5 COMPARISON WITH MODELS

6.5.1 Low-velocity systems

Phillips, Gondhalekar & Pettini (1982) and Phillips *et al.* (1984a) have shown that depletions are approximately linearly dependent (in a log–log metric) on the mean line-of-sight space density of hydrogen for a variety of elements in low-velocity clouds. Moreover, they were able to show that the strength of the dependence correlates well with the ratio of adsorption binding energy to the square root of the atomic weight, $E_{\mathrm{ads}}/A^{1/2}$. They interpreted this result in terms of a dynamic model of grain formation and destruction, where the accretion rate is higher for slower (more massive) species while the rate of removal from grain surfaces depends on E_{ads} (sputtering efficiency inversely related to adsorption energy; Barlow 1978). Our results for depletions in the low-velocity H I gas are typical of those expected for $\log\langle n(\mathrm{H})\rangle \approx -1$ (Section 5.4) on the basis of Phillip's *et al.*'s results.

We have presented evidence for partial grain destruction in the low-velocity H II region towards 50896: silicon appears to have $\delta \approx -1.2$ (as in the LV H I gas), while aluminium seems to be substantially returned to the gas phase. This would be consistent with Phillips *et al.*'s result if $\log\langle n(\mathrm{H})\rangle \lesssim -1$ for this absorption system.

In the absence of both reliable density diagnostics for the H II gas (Section 7) and an appropriate scale length for the line-forming region, we cannot prove that this differential depletion is simply a consequence of the empirical density dependences demonstrated by Phillips *et al.*, and the physical processes they propose to explain it. However, the most obvious alternative – that the two elements are differentially returned to the gas phase as a result of thermal sputtering by high-velocity particles in the H II region – seems implausible. From Barlow & Silk (1977) we estimate that a velocity of $\sim 70\,\mathrm{km\,s^{-1}}$ is required to sputter silicon – $\sim 3\times$ that required to remove aluminium from grain surfaces. Although this is in the correct sense to explain the observed effect, plausible ionic thermal velocities are of the order of a few $\mathrm{km\,s^{-1}}$, far too small to be of importance. Thermal sputtering therefore seems to be an unlikely mechanism for explaining the observed H II region depletions.

6.5.2 *High-velocity systems*

Grain destruction in high-velocity clouds has now been shown to occur for a variety of sightlines (M8 – Welsh 1983; Carina Nebula – Laurent, Paul & Pettini 1982; Welsh & Thomas 1982; Shajn 147 – Phillips, Gondhalekar & Blades 1981; Vela SNR – Jenkins, Silk & Wallerstein 1976; and several stars discussed by Cowie 1978). From these results it appears, empirically, that line-of-sight velocities in excess of $\sim 30\,\mathrm{km\,s^{-1}}$ are associated with significant grain destruction. In the -75 and $-130\,\mathrm{km\,s^{-1}}$ systems towards 50896 we have also found at least partial, and possibly total, grain destruction.

In the $-75\,\mathrm{km\,s^{-1}}$ system, for which we have the most complete data, only carbon may remain locked in grains to any significant extent (recalling, though, that C^{2+} is unobserved), while silicon appears to be returned almost entirely to the gas phase (Fig. 11). This is qualitatively consistent with the models of shock processing of interstellar grains given by Seab & Shull (1983; SS83), in which silicates are seen to be rather fragile, while graphite is the most durable grain material. A quantitative comparison with SS83's results is therefore of interest. Although their initial grain composition is mildly inconsistent with the depletions given in Table 7(a), the most significant differences are for C, N, and O (Fig. 11), which, as we have noted, are the very elements most likely to have their abundances underestimated in the gas phase; any revisions would probably improve agreement. (In any case, there is no *a priori* reason to suppose that the present grain composition derived for the LV H I medium represents a better initial boundary condition for the $-75\,\mathrm{km\,s^{-1}}$ system than the abundances adopted by SS83.)

The observations are confronted with SS83's results in Fig. 11, which shows excellent agreement between the model calculations (for a shock velocity of $80\,\mathrm{km\,s^{-1}}$) and the empirical abundances. If anything, grain destruction may have taken place to a slightly greater extent than predicted, but the differences are well within the leeway allowed by uncertainties in the observations, in the initial grain composition, and in the possible corrections required to convert line-of-sight to space velocities. We conclude that shock processing provides a satisfactory explanation for abundances in the $-75\,\mathrm{km\,s^{-1}}$ absorption system. (We note, incidentally, that the normalized extinction curve predicted for the remnant grain composition differs insignificantly from the 'standard' prescription.)

7 Density estimates

As shown in Section 6.1, the electron density in the H^0 gas can be roughly estimated from the observed ionization balance of, say, magnesium, if the radiation field is assumed. Rather more firm density estimates can in principle be obtained from populations of collisionally excited fine-structure levels. Considerable errors may still arise from the (certainly wrong) assumption that different species share the same constant density space distribution along the line-of-sight, although we do obtain numbers which are at least internally consistent for the low-velocity neutral gas.

Table 8. Density estimates. C^+ is formed in both H I and H II regions, and so density estimates based on C II*/C II are given assuming both electron and neutral hydrogen excitation.

Species	LV H I	LV H II	-75	-130	Notes
C I*/C I	2.2±0.2	...	...	...	Log $n(H^0)$, T = 30-300K
C I**/C I	2.4±0.4	...	...	...	Log $n(H^0)$, T = 30-300K
C II*/C II	2.5±0.7	...	...	...	Log $n(H^0)$, T = 3×10^2-3×10^4K
C II*/C II	...	0.8±0.8	...	...	Log n_e, T = 10^2-3×10^4K
C II*/C II	...	...	1.9±0.4	...	Log $n(H^0)$, T = 10^2-3×10^4K
C II*/C II	...	...	0.0±0.4	...	Log n_e, T = 10^2-3×10^4K
C II*/C II	...	...	...	<2	Log $n(H^0)$
C II*/C II	...	...	...	<0	Log n_e
N II*/N II	...	...	-1.1±0.4	...	Log n_e, T = 10^2-10^4K
N II**/N II	...	-0.6±0.3	...	...	Log n_e, T = 10^2-10^4K
Mg II/Mg I	-1.2:	...	...	...	Log n_e

Results are summarized in Table 8 where, for convenience, we have adopted the statistical equilibrium calculations published by Smeding & Pottasch (1979). Since C^0 is principally an H I region ion, while N^+ is principally an H II region ion, we have assumed the dominant excitation mechanisms to be impacts with neutral hydrogen and electrons, respectively. Results for both processes are given for C^+, which can occur in both neutral and H II regions; however, comparison with the C^0 data suggests that it is principally an H^0 ion in the low-velocity gas.

Given that $\log N(H^0)\approx20.7$ and that $\log n(H^0)\approx2.2$ in the low-velocity neutral hydrogen system (Section 5, Table 8), the characteristic scale length, L, of clouds along the line-of-sight must be of order ~1 pc. We could, in principle, apply a similar argument to the ionized gas; however, it is known that N II diagnostics can give anomalously low density estimates, for reasons not fully understood (e.g. Jenkins, Silk & Wallerstein 1976). Also, it is not immediately clear why N II** should be detected in the low-velocity gas while N II* (which should have a column density ~10×greater) went unreported by Shull (1977). [For completeness only, we note that the nitrogen line ratios give $L(H^+)\sim50$ pc in the LV H II gas, while for the $-75\,\mathrm{km\,s^{-1}}$ system $L(H^+)\lesssim8$ pc.]

8 The interstellar environment of HD 50896

8.1 THE FIELD STARS

The sightline to 50896 is evidently quite complex even at the resolution afforded by *IUE*. Plate 1, adapted from Chu *et al.* (1982), shows the region of southern Canis Major in which 50896 lies, and illustrates the grouping of H II nebulae in this area (see Chu *et al.* for details). In an attempt to better understand this region of space, and the origin of the absorption systems seen in our data, we have examined the UV spectra of a number of stars close to 50896 on the plane of the sky (Section 2.4; Table 2). Plate 1 and Fig. 12 show the locations of these stars. All these observations were secured from the *IUE* archives; most were originally obtained by R. A. Fesen, J. N. Heckathorn, and W. Schmutz, in part with the purpose of investigating some of the questions addressed in the present paper.

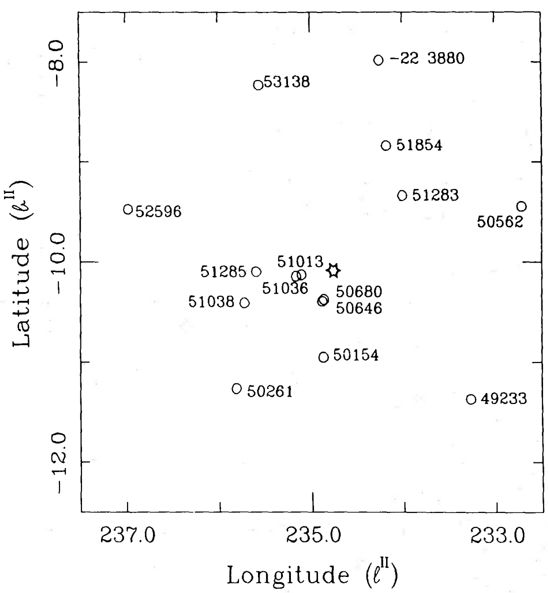

Figure 12. The locations of stars near HD 50896 (represented by the unlabelled starred circle near the centre of the figure).

Table 9. Field star data. Full details are given in the text (Section 8.2).

Star	V	H Col. (dex/cm²)	E(B-V) (a)	(b)	(c)	(d)	Arithmetic Mean	Spectral type (e)	(f)	(g)	Distance (kpc) (j)	(k)	(l)	(m)	Geometric Mean
49233	8.28	20.6	...	0.014	0.02	0.01	0.015	B3.5	dB3	B3 V	...	0.75	0.99	1.02	0.91
50154	8.93	20.8	0.022	0.015	0.03	0.01	0.019	B3.3	dB2.5	B3 V	1.10	1.02	1.38	1.56	1.25
50261	...	20.7	...	...	0.00	0.01	0.005	B5.9	dB3	...	...	...	0.76	1.22	0.96
50562	8.64	...	0.172	0.180	0.13	0.16	0.160	B7.0	...	...	2.12	1.80	0.65	...	1.35:
50646	7.71	20.4	0.019	0.009	...	0.01	0.013	...	dB2	B1 V	1.03	0.90	...	1.40	1.09
50680	8.27v?	20.5	0.016	...	...	0.01	0.013	...	dB2	...	1.26	...	...	1.42	1.34
51013	8.30	20.7	0.018	...	...	...	0.018	...	dB3	...	0.80	...	...	1.21	0.98
51036	8.80	20.35	0.034	0.015	0.00	0.01	0.015	B4.1	dB3	...	1.57	0.95	1.03	1.29	1.19
51038	9.12	20.85	0.019	0.024	0.00	0.01	0.013	B5.3	dB3	B3 V	1.11	1.16	0.95	1.50	1.16
51283	5.32	20.2	0.046	0.048	0.04	0.01	0.036	B2.5	gB2	B3 II-III	0.99	0.62	0.75	0.57	0.72
51285	8.20	20.4	0.047	0.053	0.06	0.09	0.062	B2.0	dB1.5	B2 V*nn*	2.37	2.34	1.47	1.59	1.90
51854	8.89	20.5	0.070	0.062	0.07	0.09	0.073	B1.0	dB1.5	B2 V	1.79	1.74	3.35	2.16	2.18
52596	7.36	20.55	...	0.055	0.05	0.01	0.038	B2.3	dB2.5	B3 V	...	0.61	0.93	0.74	0.75
53138	3.04	20.25	...	0.000	0.02	0.01	0.010	B3.7	sB3	B3 Ia	...	1.12	1.04	0.70	0.93
-23 3880	9.91	20.9	...	...	...	0.16	0.16:	...	dB1	...	...	...	...	3.8	3.8±
50896	(6.94)	20.7	...	...	...	0.10	0.10	...	...	WN 5	...	...	...	...	2.0±

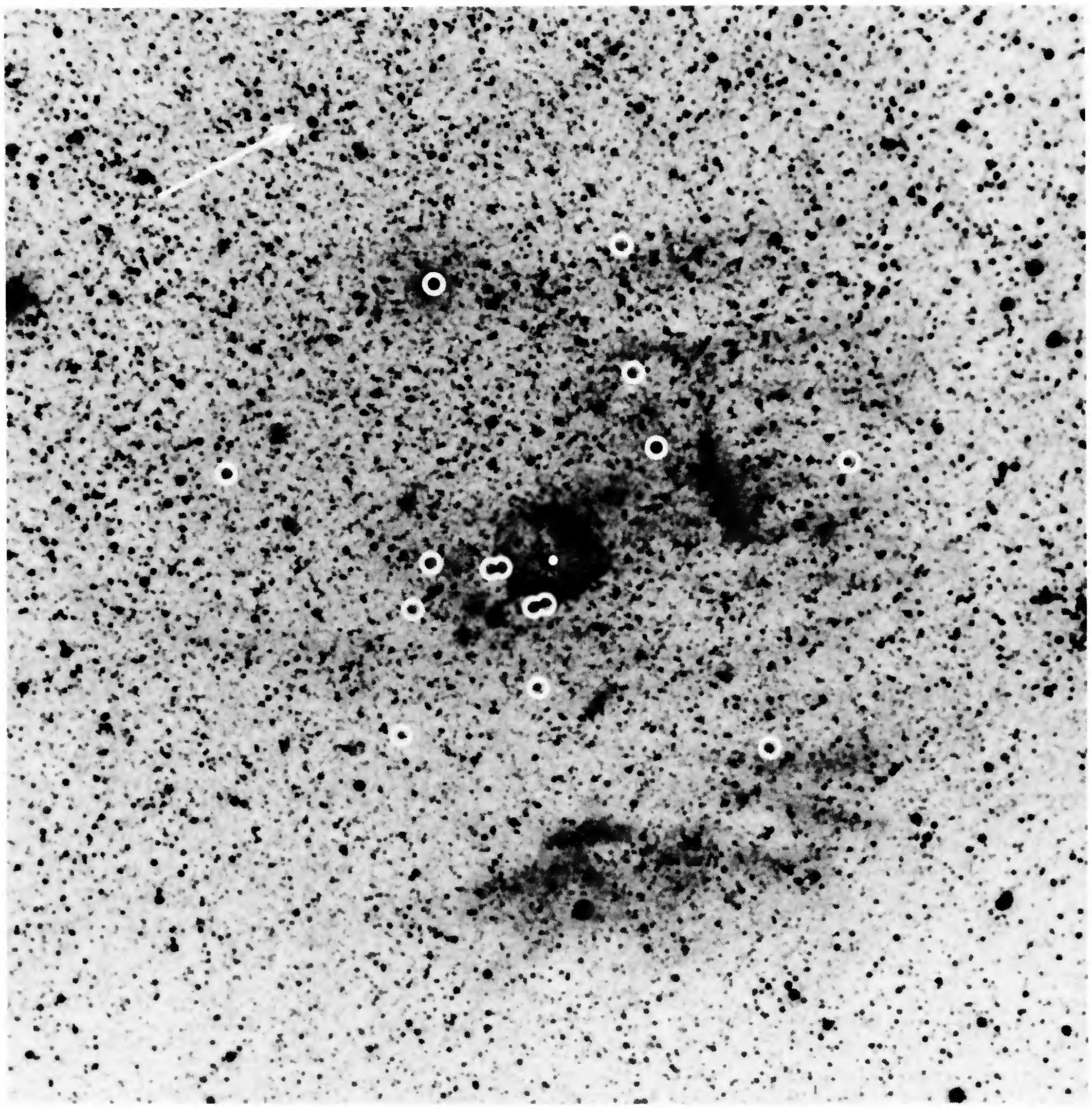

Plate 1. The sky around HD 50896, showing regions of [O III] emission. This print is from an original plate described by Chu *et al.* (1982), who also give a much deeper print showing the full extent of the nebulosity. HD 50896 is shown as a filled dot; the circled stars, which are discussed in Section 8, are identified in Fig. 12. The line at top left is one degree long and points north.

[*facing page* 838]

8.2 ASTROPHYSICAL PARAMETERS

Table 9 summarizes some useful astrophysical data for the field stars observed with *IUE*. Strömgren photometry for many of them has been published by Eggen (1981) and Kilkenny (1978, 1981). The quoted V magnitudes are from these sources (assuming $V=y$) excepting HD 51283 and 53138 (Strömgren photometry from Hauck & Mermilliod 1980), CD −22 3880 (*UBV* from Deutschman, Davis & Schild 1976), and HD 50896 (Smith v from Lundström & Stenholm 1984). Reddenings and distances have been estimated from the same data following Moon & Dworetsky (1985, using programs from Moon 1985); columns (a) & (j) and (b) & (k) (Table 9) give results from Eggen's and Kilkenny's photometry, respectively.

Hydrogen columns have been estimated from Ly-α, assuming a flat continuum. (This may overestimate columns for later B types, which have broad intrinsic features, but is probably not a problem in the present sample.) They are believed to be accurate to ± 0.2 dex or better.

The reddenings and (one-dimensional) spectral types can be estimated from S2/68 UV spectrophotometry. D. J. Carnochan (personal communication) has provided best (least-squares) estimates of these parameters from specially reprocessed data, and these are also entered in Table 9 [columns (c) and (e)]. [Luminosity class V was assumed in the fitting process unless a different classification is quoted in column (g) of Table 9.] Although the spectra are quoted to a tenth of a sub-type, this a purely formal result; the results are probably accurate to ~1 sub-type (see Carnochan 1986 for details).

The high-resolution *IUE* spectra can provide estimates of differential reddenings, by ratioing the data and taking out the 2200 Å bump in the usual way; these results are put on an absolute basis by scaling to stars with known reddenings, and are given in column (d). The *IUE* spectra also provide quite good estimates of (two-dimensional) spectral types [column (f)], following the scheme of Heck *et al.* (1984), which appears to correspond quite closely to the MK classification. Results are again believed to be accurate to ~1 sub-type.

Finally, MK spectral types are available in the literature for a number of stars. Classifications in column (g) of Table 9 were taken from (in decreasing order of preference) Dworetsky, Whitelock & Carnochan (1982; HD 49233, 50154, 51285, 51854, 52596); Hiltner & Morgan (1969; 53138); Morgan, Code & Whitford (1955; 51283); Heckathorn & Fesen (1984; 50646, 51038); and Van der Hucht *et al.* (1981; 50896). The spread in spectral type for the sample is quite small, due largely to selection effects.

Distances follow from the photometry as noted above [columns (j), (k)]. The flux levels of the S2/68 data, together with the corresponding spectral-type estimates and reddenings, and the intrinsic parameters compiled by Carnochan (1982), give independent self-consistent distance estimates for each star [column (l)]. Finally, the adopted reddenings and visual magnitudes can be used with the spectral types of column (g) [or (f)] and Carnochan's (1982) data to give a fourth measurement of distance [column (m)]. For HD 50261, which has no photoelectric visual magnitude available, the normalization was done by scaling from the observed $\lambda\lambda$1750–1850 fluxes (in *IUE* FN/s) of other targets. For CD −22 3880 it seemed worthwhile to use Johnson *UBV* photometry to provide a check on the results from the *IUE* data. Taking colours from Deutschman *et al.* (1976) we find $Q=-0.70$, corresponding to a spectral type of ~B1.5 V (or B2.5 III) and $E(B-V)=0.16$ (Carnochan 1982), and a distance of 3.0 (or 3.5) kpc. There can be little doubt that this star is the most remote in our sample.

The distances in columns (j)–(m) of Table 9 show no significant systematic differences, although values for individual stars are evidently uncertain by ~20 per cent or more. Most objects clearly fall at the ~1 kpc distance of the ill-defined Cr 121 cluster (see Eggen 1981); apart from a small handful of apparently rather more distant stars (HD 51285 and 51854, CD −22 3880) the scatter in the adopted distances is entirely consistent with the hypothesis of equidistance when allowance is made for the unexpected uncertainties of ~1 sub-class in the adopted spectral types.

The three most distant ($D \gtrsim 1.5$ kpc) stars have slightly larger reddenings than the remainder of the sample. Although the reddenings are too small, and the sightline too poorly sampled in terms of distances, to construct a reliable D versus $E(B-V)$ diagram, this datum does hint at a distance in excess of ~1.5 kpc for 50896, if our estimate of its reddening (Section 5) is reliable.

Table 10. Selected measurements of interstellar lines towards field stars, in mÅ. Ellipsis dots are given where a line is absent or unmeasurable (e.g. because of inseparable blending with photospheric features); braces mean that different velocity components could not be measured individually. All velocities are with respect to the low-velocity (LV) components.

Star	Vel.	1335.7	1548.2	1550.8	2795.5	2802.7	2852.1
49233	LV	107±25	34±21	19±18	456±57	378±49	190±37
50154	LV	...	61±30	58±28	421±94	414±91	182±42
50261	LV	333±32:	79±28	6±24	610±46	512±44	212±42
50562	LV	...	...	...	{1237±247	1144±229}	360±29
	-30?	...	...	...			...
	-65	...	...	...			...
50646	LV	...	64±17	63±17	510±37:	459±36:	182±36
	-80	...	...	...	271±32:	252±34:	...
50680	LV	107±12	21±10	17±9	433±65	391±60	218±40
	-80	27±11	...	...	268±43	246±40	...
	-135	...	...	...	173±32	62±18	...
51013	LV	86±22	50±28	40±30	418±41	386±41	183±38
	-85	...	...	...	...	264±40	...
51036	LV	289±62	150±75	65±32	514±31	462±29	201±28
	-85	...	...	...	267±25	226±29	...
51038	LV	...	57±28	29±28	517±39	438±37	178±32
	-100	22±17	...	...	116±39	123±33	...
	-185	...	...	...	67±31	17±28	...
51283	LV	94±22	47±30	11±28	449±38	392±34	190±38
51285	LV	216±22	32±27	44±29	649±64	578±57	267±50
	-80	...	...	...	{482±64	301±59}	...
	-110	...	...	...			...
51854	LV	216±19	51±25	24±20	{980±111	894±103}	333±30
	-70	25±15	...	...			...
52596	LV	...	122±40	69±32	533±51	400±49	242±47
53138	LV	138±12	16±21	20±20	927±30	859±31	194±21
	-150	...	...	...	210±22	71±20	...
-22 3880	LV	...	302±65	204±59	667±69	774±72	572±72

8.3 THE INTERSTELLAR LINES

Measurements of interstellar line strengths for a range of ions have been made in all the spectra; selected results are given in Table 10. Since almost all the stars for which UV spectra are available are early B main-sequence objects, they exhibit rich photospheric spectra with comparatively narrow lines. This makes the measurement of interstellar lines comparatively difficult (and for some features, like Si III λ1206, virtually impossible). Where necessary, systematic errors in continuum placement have therefore been assigned (in an *ad hoc* fashion) when evaluating the uncertainties on equivalent-width measurements (see Appendix I).

Several important conclusions follow immediately from inspection of the interstellar survey data. First, many of the stars observed are seen through the $-75\,\mathrm{km\,s^{-1}}$ component already identified in 50896. Secondly, several stars show evidence for additional high-velocity absorption systems (at up to $-185\,\mathrm{km\,s^{-1}}$ in HD 51038). Finally, none of the spectra studied exhibit lines from H II region species at anywhere near the strength of those seen towards 50896, with the exception of CD −22 3880.

The absence of H II gas at high velocities in the field star spectra is consistent with their comparatively poor S/N ratios; we would not expect to detect C IV and Si IV if they were present with strengths not exceeding those in 50896. However, C IV and Si IV lines as strong as those seen in 50896 at low velocity and/or $-30\,\mathrm{km\,s^{-1}}$ should certainly be seen. Our basic conclusion is, therefore, that there are no major differences between 50896 and many of the field stars in respect of the higher velocity systems, but that observations of 50896 are unique in showing strong H II region lines at $-30\,\mathrm{km\,s^{-1}}$. Its LV H II system is also exceptional, but shares some characteristics with the sightline to CD −22 3880.

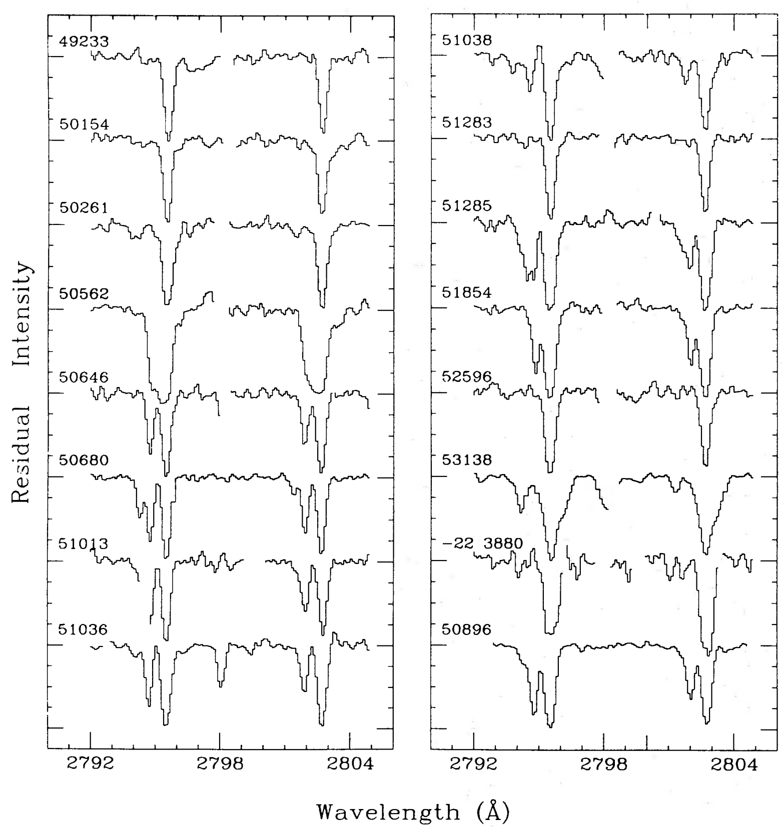

Figure 13. Rectified profiles of the Mg II λ2800 doublet in the spectra of stars in southern CMa. Continuum and zero levels are marked for each spectrum.

The strongest lines in all the spectra are those due to the Mg II λ2800 doublet. A montage of these features towards all stars studied is given in Fig. 13, and illustrates the widespread occurrence of high-velocity features. [HD 50646, 51036, 51038, and 53138 apparently show a velocity system at $\sim -500\,\mathrm{km\,s^{-1}}$; these lines are in fact attributable to (photospheric) Mg II $3p\,^2P^0$–$3d\,^2D$, although their relationship to the stellar spectral type is ambiguous.]

We now turn to a further discussion of the major velocity systems in the light of these results.

9 Discussion

In this section we review the nature of each of the absorption systems observed towards 50896, excluding the low-velocity H I complex, which has no particularly noteworthy characteristics in our data, and which has previously been discussed in detail by Shull (1977).

9.1 THE LOW-VELOCITY H II GAS

Exceptionally strong absorption from H II region species appears to be a rather common characteristic of UV WR spectra. In particular, Smith *et al.* (1980) found that six out of 10 WR stars they studied show remarkably strong Si IV and C IV absorption lines.

Two of these six stars lie in the Carina complex, an extremely active region where a number of O stars show similar features (Laurent *et al.* 1982; Welsh & Thomas 1982). For a further three stars (leaving only 50896) Smith *et al.* attributed the strong lines from ionized gas to absorption in the Cygnus loop. In fact the stars concerned (HD 191765, 192103, and 192163) do not lie in the same direction as that SNR, but they are in the direction of Cyg OB1, where again a number of O stars show very strong C IV and Si IV interstellar lines (Phillips, Welsh & Pettini 1984b). It therefore seems likely that, as suggested by Smith *et al.*, the greater part of the ionized gas they reported towards these five Wolf–Rayets arises in large-scale distributed structures in the interstellar medium, rather than in material directly associated with the stars themselves.

In the case of 50896, no nearby OB association is available to power an active local ISM. Smith *et al.* attributed the low-velocity H II gas in this sightline to the ring nebula S308, but the rather large column of gas involved, and the interpretation given in Section 9.2, argue against this. We therefore suggest an H II region local to, and powered by, 50896 as being responsible for the great strength of highly ionized interstellar species seen towards this star. Smith *et al.* considered this possibility, but dismissed it on the grounds that model calculations for stars of $T_{\mathrm{eff}} \approx 3\times10^4$ K (and normal H-rich atmospheres) fail to produce sufficiently strong lines. However, there is evidence that the emergent far-UV radiation fields of at least some WR stars are characterized by much higher temperatures than was generally believed until recently (Hillier 1983; Cherepashchuk, Eaton & Khaliullin 1984). Some rough calculations reported in Appendix II suggest that Helium-rich atmosphere with an effective temperature of $\approx$65 000 K can maintain the level of ionization required to explain the C IV, Si IV, and other H II region species seen at low velocity towards 50896.

If this is the correct explanation, then the problem arises as to why some WRs do *not* show strong absorption. Although the number of stars sampled is not very large, Smith *et al.* found no correlation of absorption equivalent width with spectral type, suggesting that a simple temperature effect is not responsible. Differences in the density of the local interstellar medium may therefore be contributory; or it may be that the WR sub-types do not indicate a temperature sequence, a possibility that would be 'scary but not surprising' (Conti 1986). Conversely, it is worth noting the exciting possibility that if the strong lines of highly ionized species do indeed arise in H II regions local to at least some WR stars, and if reliable estimates of the density of absorbing gas can be made, then available observations of interstellar lines (or new observations of nebular emission spectra), together with trivial modelling of the radiative transfer, may provide a powerful probe of that essentially unknown quantity, the emergent far-UV radiation field of a Wolf–Rayet star.

HD 50896 appears to be the only star capable of exciting the complex of H II regions shown in Plate 1 (Chu *et al.* 1982). Since strong C IV and Si IV absorption is seen in the spectrum of the WR, it must lie within (or beyond) the observed nebulosity, if we identify the latter with the line-forming gas. At the same time, the nebulae must be beyond all the HD stars listed in Table 9, since none of these show strong H II region absorptions; in particular, the C IV lines seen towards the relatively distant HD 51285 and 51854 are quite unremarkable. (It might be supposed that photons capable of ionizing C^{2+} do not penetrate to the angular distance of, for example, 51854 from 50896, but the presence of moderately strong C IV absorption towards CD −22 3880 argues that this is not so.) These results give a firm basis for the belief that the absorbing region (and hence 50896) lies beyond HD 51285 and 51854, while if 50896 were significantly more distant than CD −22 3880 it would be improbably luminous; in other words, D=2–3 kpc.

9.2 THE $-30\,\mathrm{km\,s^{-1}}$ SYSTEM

Chu *et al.* (1982) have reported Fabry–Perot observations of the emission lines formed in S308, finding that the nebula can be roughly represented by a uniformly expanding shell with an expansion velocity of $\sim 60\,\mathrm{km\,s^{-1}}$ and a systemic velocity of $+30\,\mathrm{km\,s^{-1}}$ (LSR). In the observer's velocity frame adopted in this paper the velocity of gas seen in projection against the star is, therefore, expected to be $\sim -40\,\mathrm{km\,s^{-1}}$. Given the uncertainties in relating our velocity scale to that of the Fabry–Perot data, it seems very likely that the $-30\,\mathrm{km\,s^{-1}}$ absorption system identified in the 50896 sightline arises in S308.

Simple geometry shows that the equivalent hydrogen column density for a spherical nebula lies in the range

$$N(\mathrm{H})=\left\{(18.3\text{–}18.8)+\log_{10}\left[\left(\frac{2\,\mathrm{kpc}}{D}\right)^2\left(\frac{M_{\mathrm{neb}}}{30\,M_\odot}\right)\right]\right\}\ \mathrm{dex\,cm^{-2}},$$

depending on whether the gas uniformly fills the sphere or is confined to a thin shell. The parameters chosen represent the adopted distance and (very poorly known) mass of S308 (Section 5.4; Kwitter 1984). Consistency with the hydrogen column estimated for the observed absorption system (Section 5.4) provides further support for interpreting this system as arising in the nebula.

If the absorption system has been correctly identified, then it is only the second attributable to a WR ring nebula. The other, RCW 58 (towards HD 96548), has a similar hydrogen column density, but otherwise shows very different characteristics (Smith *et al.* 1984): a velocity offset of $\sim -125\,\mathrm{km\,s^{-1}}$, and a substantial velocity gradient of $\sim 50\,\mathrm{km\,s^{-1}}$ which is certainly absent in S308. Dyson & Smith (1985) have emphasized the heterogeneity of WR ring nebulae, and so perhaps these differences are not surprising. In particular, direct imaging of RCW 58 shows a highly structured series of radially directed filaments and clumps (Chu *et al.* 1982; J. L. Smith, personal communication), while S308 is one of the more uniform and regular of the known galactic WR ring nebulae. These morphological differences suggest that whereas RCW 58 is dominated by stellar ejecta (Smith *et al.* 1984), S308 may more nearly represent a 'simple' wind-blown shell whose characteristics are determined principally by the swept-up interstellar medium.

A note of caution has to be sounded. One of the stars in our survey, HD 50562, appears to have absorption at intermediate velocities between the low-velocity and $-75\,\mathrm{km\,s^{-1}}$ features (Fig. 13).

If this absorption is attributable to the same gas as that giving rise to the $-30\,\mathrm{km\,s^{-1}}$ component in 50896, then it is obviously *not* formed in S308. Unfortunately 50562 is the only star considered here for which SWP data are unavailable, and we cannot, therefore, discuss a possible H II region spectrum. Furthermore, its distance appears not to be very reliably established (Table 9). We note, however, that HD 51285 and 51854 have smaller angular separations from 50896 and are almost certainly more distant than 50562, and yet they do not show evidence for the strong intermediate-velocity absorption seen in that star. This makes it unlikely that it is the same gas that is responsible for this absorption in both 50896 and 50562.

HD 50680 lies just inside S308 as seen on the sky. Given that the $-30\,\mathrm{km\,s^{-1}}$ component in 50896 does arise in that nebula, the absence of detectable absorption at this velocity in 50680 (including the lack of strong Si IV and C IV lines) gives further evidence that 50896 is more distant than about 1.3 kpc.

9.3 HIGHER VELOCITY SYSTEMS

As noted in the introduction, the $-75\,\mathrm{km\,s^{-1}}$ system has generally been interpreted as arising in S308. However, the simple observation that it is present across some 3 or more degrees of sky (compared to the ~30 arcmin diameter of S308) immediately rules this out as being the correct explanation.

The presence of the $-75\,\mathrm{km\,s^{-1}}$ component in HD 50562, 51854, 50896, and a number of stars at ~1 kpc, but not in 51283, constrains the distance of the absorbing gas to be ~0.8 (±0.2) kpc (unless we view 51283 through a 'hole' in the gas, in which case the line-forming region could be substantially closer to us). Its full angular extent is not adequately defined by the present data, but the absence of absorption in the spectra of −22 3880 and 50154 suggests ~3–4 degrees, or ~50 sec i pc (where i is the angle made by the major axis of the material to the plane of the sky). The gas density is very uncertain, but for $\log n(\mathrm{H}) \gtrsim -1$ (Table 8) and $\log N(\mathrm{H}) = 18.3$ (Section 5) the characteristic thickness of material is $\lesssim 10/\sec i$ pc (and probably ~1 pc), so we can safely state that we are looking through a sheet, rather than a roughly spherical cloud, of gas. Substantial differences in the line profiles of the highest velocity features can exist in stars as close together in the plane of the sky as HD 50646 and 50680 (Fig. 13), separated by only ~3 arcmin, implying structure on scales at least as small as $0.7\,(D/0.8\,\mathrm{kpc})/\sec i$ pc.

Similar high-velocity absorption systems have been reported in several sightlines on the basis of ultraviolet data: e.g. the I Per OB association (Phillips & Gondhalekar 1981; McLachlan & Nandy 1085), the Carina Supershell (Laurent *et al.* 1982), Cyg OB1 (Phillips *et al.* 1984b), and Ori OB1 (Cowie, Songaila & York 1979). At least three possible explanations can be put forward for their occurrence. The first, thermal expansion of an H II region, can be ruled out in general because the velocities are very much greater than expected. A second explanation, which appears to be consistent with observations of at least some of the OB associations mentioned above, is that expansion is powered ultimately by the winds of early-type stars. This is unlikely to be the correct explanation in the present case, since the bubble associated with 50896 has been separately identified (S308, at $-30\,\mathrm{km\,s^{-1}}$) and there are no other early-type stars in the vicinity with sufficiently strong winds to drive a bubble nebula of the scale observed.

The third possibility, which seems to us to be the most convincing, is that the $-75\,\mathrm{km\,s^{-1}}$ feature arises in an old supernova remnant (SNR). This interpretation offers a natural explanation for the additional high-velocity systems ($|v| \gtrsim 10^2\,\mathrm{km\,s^{-1}}$) seen towards 50896 and nearby field stars, and the differences between them, since the most recent and physically complete models of SNRs have emphasized that secondary, and multiple, shock structures are expected to be typical, rather than exceptional, and that the nature of the secondary shocks depends critically on the microstructure of the ISM through which the blast wave has passed

(Innes, Giddings & Falle 1985; Innes 1985). This suggests that the multiple absorption systems seen in several sightlines can be explained as the consequence of a single supernova, without having to make recourse to *ad hoc* multiple events or implausible geometries. [Heckathorn & Fesen (1984) also concluded that high-velocity features in this region of sky arose in an SNR, but put a somewhat different interpretation on the velocity systems observed.]

A possible objection to an SNR origin for the high-velocity absorption systems is that the systematic velocity gradients expected to arise from projection effects when looking through different parts of a spherically expanding shell are not seen. It may simply be that we have no observations close enough to the edge of the shell to reveal such effects, but it should be noted that projection effects are also absent towards the well-studied Vela SNR (Jenkins *et al.* 1984). The Vela SNR also has in common with the CMa sightline a striking absence of high-velocity Al III absorption; this is probably attributable to non-equilibrium ionization in the line-forming region (Jenkins *et al.* 1984).

Simple energetics support an SNR origin for the high-velocity systems. From Chevalier (1974) we have

$$E_{50}=5.3\times10^{-7}\left(\frac{R}{\mathrm{pc}}\right)^{3.12}\left(\frac{V}{\mathrm{km\,s^{-1}}}\right)^{1.40}\left(\frac{n_0}{\mathrm{cm^{-3}}}\right)^{1.12},$$

where R is the SNR radius, V the shock velocity, n_0 the number density, and E_{50} is the initial energy in units of 10^{50} erg. Substituting 25, 130, and 1 respectively, we obtain $E\approx51.0$ dex erg, in satisfying agreement with the value of 51 canonically considered appropriate for a Type II SN; using $V=75\,\mathrm{km\,s^{-1}}$ gives $E=50.7$ dex erg, leaving this conclusion unaffected. (Of course, the shock velocity will actually be greater than the observed absorption-line velocity, but any error arising from this is likely to be smaller than that due to uncertainties in the density.)

The observed velocities imply temperatures of order $\sim10^5$ K, just cool enough to be consistent with Shull's failure to detect O VI absorption towards 50896. The corresponding thermal motions lead to b values of order $10\,\mathrm{km\,s^{-1}}$, also consistent with the observations. A velocity gradient of order $\sim$10–20 $\mathrm{km\,s^{-1}}$ is expected through the cooling zone on the basis of simple models (*cf.* McCray & Snow 1979), and a search for such a gradient across different ions – and for the presence of differences in line profiles – should be undertaken when better resolution becomes available in the UV. More detailed modelling is also clearly desirable, to see if features like the diffuse soft (M-band) X-ray emission from this direction (visible in the data of McCammon *et al.* 1983) and the absence of detectable radio emission (Chu *et al.* 1982) can be quantitatively explained on the basis of an SNR model.

9.4 A NEUTRON STAR COMPANION TO 50896?

Speculation naturally arises as to the progenitor of the remnant discussed here. Since we have concluded that it is at a distance of 0.8 ± 0.2 kpc, with a radius of $\sim$25 pc, two possibilities suggest themselves. The first is that it is the remnant of a massive star formed coevally with the B stars still present in Cr 121; the rather more interesting alternative is that the SNR is associated with HD 50896. As noted in Section 1, there has been much discussion about the possible existence of a neutron star companion to WR star, and the positive association of an SNR with the Wolf–Rayet would add considerably to the plausibility of such a companion.

Taken at face value, the lack of definite absorption systems at positive velocities in the spectrum of 50896 places it firmly inside any spherically symmetric structure. Unfortunately, that such systems are also absent in the spectra of relatively distant stars, which should be behind the SNR (HD 51285 and 51854), suggests that spherical symmetry may not be a reasonable approximation – the 'back' of the shell may have expanded into a comparatively empty region of a space. Moreover, if 50896 is within the supernova remnant – presumably a region of low-density hot gas – then there may be some difficulty in accounting for the cold, swept-up material producing S308. Finally, and most persuasively, we have argued that the WR lies at ~2–3 kpc, and is therefore too remote to be associated with the SNR. Ultraviolet spectroscopy of more distant stars in this direction, and of stars with greater angular separations from 50896, should eventually help resolve the issue, but we believe that the balance of the available evidence argues *against* an association between 50896 and the SNR.

10 Résumé

We have produced a photometrically precise, high-resolution, UV spectrum of HD 50896 by averaging 31 individual observations, using 21 additional spectra to check the wavelength scales and to flux calibrate the data; a quantitative description of the mean spectrum has been given. We have also examined 40 spectra of 15 field stars to help us understand the interstellar medium in the line-of-sight towards 50896.

Our principal conclusions are:

(i) Depletions in the low-velocity H I system in this direction are unexceptional.

(ii) Strong lines seen at low velocity in the spectrum of 50896, and arising from highly ionized (IP>13.6 eV) species, are probably formed in an H II region associated with the WR star, at a distance of ~2–3 kpc.

(iii) A barely resolved absorption system, blueshifted from the low-velocity gas by ~30 km s^{-1}, is attributable to the ring nebula S308 associated with 50896.

(iv) High-velocity ($v \gtrsim |70|$ km s^{-1}) absorption systems seen towards several stars show evidence for substantial grain destruction. These systems are attributed to an old SNR; although this may be associated with a putative neutron star companion to 50896, the available evidence argues against this conclusion.

A better understanding of this region of space requires UV observations with higher sensitivity and resolving power than are available at the time of writing, and a self-consistent model of the mooted SNR.

Acknowledgments

This paper embodies part of the research carried out in the UV group at UCL under the leadership of Professor R. Wilson, whose support is warmly acknowledged. The work would not have been possible without the facilities offered by STARLINK, and by the *IUE* Project staff at the Rutherford Appleton Laboratories. IDH wishes to thank Allan Willis for several interesting discussions on the problems of 50896's spectrum, John Hillier and Werner Schmutz for access to unpublished material, You-Hua Chu for the generous loan of the original plate used to produce Plate 1, and Jack Giddings and Davina Innes for trying to teach him that supernova remnants really aren't that simple. Dave Carnochan kindly provided special de luxe versions of S2/68 data, and software to manipulate them, and Robin Clegg gave tutorials on how to run the Harrington photoionization code. Special thanks are due to Linda Smith, who gave us permission to quote unpublished results, offered many helpful suggestions, and encouraged us to complete this work after it had lain fallow for several years. APP was supported by a SERC Research Fellowship.

References

Abbott, D. C., 1978. *J. Phys. B*, **11**, 3479.
Abbott, D. C., Bohlin, R. & Savage, B. D., 1982. *Astrophys. J. Suppl.*, **48**, 369.

Abbott, D. C., Bieging, J. H., Churchwell, E. & Torres, A. V., 1986. *Astrophys. J.,* **303,** 239.

Ake, T. B., 1981. *NASA IUE Newsletter No. 15,* p. 60.

Barlow, M. J., 1978. *Mon. Not. R. astr. Soc.,* **183,** 417.

Barlow, M. J. & Silk, J., 1977. *Astrophys. J.,* **211,** L83.

Bianchi, L. & Bohlin, R., 1983. *ESA IUE Newsletter No. 16,* p. 17.

Boggess, A. *et al.*, 1978. *Nature,* **275,** 372.

Bohlin, R. C., Savage, B. D. & Drake, J. F., 1978. *Astrophys. J.,* **224,** 132.

Carnochan, D., 1982. *Mon. Not. R. astr. Soc.,* **201,** 1139.

Carnochan, D., 1986. *Mon. Not. R. astr. Soc.,* **219,** 903.

Cassatella, A., Barbero, J. & Benvenuti, P., 1985. *Astr. Astrophys.,* **144,** 335.

Cassatella, A., Ponz, D. & Selvelli, P. L., 1981. *ESA IUE Newsletter No. 10,* p. 31.

Cherepashchuk, A. M., Eaton, J. A. & Khaliullin, Kh. F., 1984. *Astrophys. J.,* **281,** 774.

Chevalier, R. A., 1974. *Astrophys. J.,* **188,** 501.

Chu, Y.-H., Gull, T. R., Treffers, R. R., Kwitter, K. B. & Troland, T. H., 1982. *Astrophys. J.,* **254,** 562.

Clavel, J., Gilmozzi, R. & Prieto, A., 1985. *ESA IUE Newsletter No. 23,* p. 48.

Clegg, R., Harrington, J. P., Barlow, M. J. & Walsh, J. R., 1986. *Astrophys. J.,* submitted.

Conti, P. S., 1986. *Luminous Stars and Associations in Galaxies, IAU Symp. No. 116,* p. 279, eds de Loore, C. W. H., Willis, A. J. & Laskarides, P. G., Reidel, Dordrecht, Holland.

Cowie, L. L., 1978. *Astrophys. J.,* **225,** 887.

Cowie, L. L. & Songaila, A., 1986. *Ann. Rev. Astr. Astrophys.,* **24,** in press.

Cowie, L. L., Songaila, A. & York, D. G., 1979. *Astrophys. J.,* **230,** 469.

Davenhall, C., 1977. *UCL internal memo, Everything you wanted to know about the new CoG program but were afraid to ask.*

Deutschman, W. A., Davis, R. J. & Schild, R. E., 1976. *Astrophys. J. Suppl.,* **30,** 97.

Dufton, P. L., Hibbert, A., Kingston, A. E. & Tully, J. A., 1983. *Mon. Not. R. astr. Soc.,* **202,** 145.

Dworetsky, M. M., Whitelock, P. A. & Carnochan, D., 1982. *Mon. Not. R. astr. Soc.,* **200,** 445.

Dyson, J. E. & Smith, L. J., 1985. *Cosmical Gas Dynamics,* p. 173, ed. Kahn, F. D., VNU Science Press.

Eggen, O. J., 1981. *Astrophys. J.,* **247,** 507.

Garmany, C. D., Conti, P. S. & Chiosi, C., 1982. *Astrophys. J.,* **263,** 777.

Garmany, C. D., Massey, P. & Conti, P. S., 1984. *Astrophys. J.,* **278,** 233.

Giddings, J., 1981a. *PhD thesis,* University of London.

Giddings, J., 1981b. *ESA IUE Newsletter No. 12,* p. 22.

Giddings, J., 1983a. *SERC Starlink User Note No. 37.*

Giddings, J., 1983b. *ESA IUE Newsletter No. 17,* p. 53.

Gondhalekar, P. M., Phillips, A. P. & Wilson, R., 1980. *Astr. Astrophys.,* **85,** 272.

Hamann, W.-R., 1985. *Astr. Astrophys.,* **145,** 443.

Harrington, J. P., Seaton, M. J., Adams, S. & Lutz, J. H., 1982. *Mon. Not. R. astr. Soc.,* **199,** 517.

Harris, A. W., Gry, C. & Bromage, G. E., 1984. *Astrophys. J.,* **284,** 157.

Hauk, B. & Mermilliod, M., 1980. *Astr. Astrophys. Suppl.,* **40,** 1.

Heck, A., Egret, D., Jaschek, M. & Jaschek, C., 1984. *IUE Low-Dispersion Spectra Reference Atlas – Part 1,* ESA SP-1052.

Heckathorn, J. N. & Fesen, R. A., 1984. *Future of Ultraviolet Astronomy Based on Six Years of IUE Research,* p. 207, NASA CP-2349.

Hibbert, A., Dufton, P. L., Murray, M. J. & York, D. G., 1983. *Mon. Not. R. astr. Soc.,* **205,** 535.

Hillier, D. J., 1983. *PhD thesis,* Australian National University.

Hillier, D. J., 1984. *Astrophys. J.,* **280,** 744.

Hillier, D. J., 1986. *Luminous Stars and Associations in Galaxies, IAU Symp. No. 116,* p. 261, eds de Loore, C. W. H., Willis, A. J. & Laskarides, P. G., Reidel, Dordrecht, Holland.

Hiltner, W. A. & Morgan, W. W., 1969. *Astr. J.,* **74,** 1152.

Hobbs, L. M., 1984. *Astrophys. J. Suppl.,* **56,** 315.

Howarth, I. D. & Maslen, D., 1983. *SERC Starlink User Note No. 50.*

Howarth, I. D., Prinja, R. K. & Willis, A. J., 1984. *Mon. Not. R. astr. Soc.,* **208,** 525.

Innes, D., 1985. *PhD thesis,* University of London.

Innes, D., Giddings, J. & Falle, S. A. E. G., 1985. *Cosmical Gas Dynamics,* p. 143, ed. Kahn, K. D., VNU Science Press.

Jenkins, E. B., 1986. *Astrophys. J.,* **304,** 739.

Jenkins, E. B., Silk, J. & Wallerstein, G., 1976. *Astrophys. J. Suppl.,* **32,** 681.

Jenkins, E. B., Silk, J. & Wallerstein, G., 1984. *Astrophys. J.,* **278,** 649.

Johnson, H. M., 1978. *Astrophys. J. Suppl.,* **36,** 217.
Johnson, H. M. & Hogg, D. E., 1965. *Astrophys. J.,* **142,** 1033.
Kilkenney, D., 1978. *Mon. Not. R. astr. Soc.,* **182,** 629.
Kilkenney, D., 1981. *Mon. Not. R. astr. Soc.,* **194,** 927.
Kurucz, R. L., 1974. *Smithsonian Astrophys. Obs. Spec. Rep. No. 360.*
Kwitter, K. B., 1984. *Astrophys. J.,* **287,** 840.
Lassettre, E. N. & Skerbele, A., 1971. *J. Chem. Phys.,* **54,** 1957.
Laurent, C., Paul, J. A. & Pettini, M., 1982. *Astrophys. J.,* **260,** 163.
Lucy, L. B., 1983. *Astrophys. J.,* **274,** 372.
Lundström, I. & Stenholm, B., 1984. *Astr. Astrophys. Suppl.,* **35,** 303.
McCammon, D., Burrows, D. N., Sanders, W. T. & Kraushaar, W. L., 1983. *Astrophys. J.,* **269,** 107.
McCray, R. & Snow, T. P., 1979. Ann. Rev. Astr. Astrophys., **17,** 213.
McLachlin, A. & Nandy, K., 1985. *Mon. Not. R. astr. Soc.,* **215,** 473.
Massey, P., 1984. *Astrophys. J.,* **281,** 789.
Moffat, A. F. J., 1982. *Wolf–Rayet Stars: Observations, Physics, Evolution, IAU Symp. No. 99,* p. 263, eds de Loore, C. W. H. & Willis, A. J., Reidel, Dordrecht, Holland.
Moon, T. T., 1985. *Publs Univ. Lond. Obs., No. 78.*
Moon, T. T. & Dworetsky, M. M., 1985. *Mon. Not. R. astr. Soc.,* **217,** 305.
Morgan, W. W., Code, A. D. & Whitford, A. E., 1955. *Astrophys. J. Suppl.,* **2,** 41.
Morton, D. C., 1975. *Astrophys. J.,* **197,** 85.
Morton, D. C., 1978. *Astrophys. J.,* **222,** 863.
Morton, D. C. & Smith, W. H., 1973. *Astrophys. J. Suppl.,* **26,** 333.
Mountain, M., 1985. *UKIRT Newsletter No. 13.*
Nachmann, P. & Hobbs, L. M., 1973. *Astrophys. J.,* **182,** 481.
Nussbaumer, H., Pettini, M. & Storey, P. J., 1981. *Astr. Astrophys.,* **102,** 351.
Nussbaumer, H., Schmutz, W., Smith, L. J., & Willis, A. J., 1982. *Astr. Astrophys.,* **106,** 379.
Phillips, A. P. & Gondhalekar, P. M., 1981. *Mon. Not. R. astr. Soc.,* **196,** 533.
Phillips, A. P., Gondhalekar, P. M. & Blades, J. C., 1981. *Mon. Not. R. astr. Soc.,* **195,** 485.
Phillips, A. P., Gondhalekar, P. M. & Pettini, M., 1982. *Mon. Not. R. astr. Soc.,* **200,** 687.
Phillips, A. P., Pettini, M. & Gondhalekar, P. M., 1984a. *Mon. Not. R. astr. Soc.,* **206,** 337.
Phillips, A. P., Welsh, B. Y. & Pettini, M., 1984b. *Mon. Not. R. astr. Soc.,* **206,** 55.
Savage, B. D. & Mathis, J. S., 1979. *Ann. Rev. Astr. Astrophys.,* **17,** 73.
Savage, B. D., Bohlin, R. C., Drake, J. F. & Budich, W., 1977. *Astrophys. J.,* **216,** 291.
Schiffer, F. H., 1980. *NASA IUE Newsletter No. 11,* p. 33.
Schmutz, W., 1982. *Wolf–Rayet Stars: Observations, Physics, Evolution, IAU Symp. No. 99,* p. 23, eds de Loore, C. W. H. & Willis, A. J., Reidel, Dordrecht, Holland.
Schmutz, W., 1984. *PhD thesis,* ETH Zurich.
Schmutz, W. & Hamann, W.-R., 1986. *Astr. Astrophys.,* submitted.
Seab, C. G. & Shull, J. M., 1983. *Astrophys. J.,* **275,** 652.
Seaton, M. J., 1979. *Mon. Not. R. astr. Soc.,* **187,** 73P.
Sharpless, S., 1959. *Astrophys. J. Suppl.,* **14,** 257.
Shull, J. M., 1977. *Astrophys. J.,* **212,** 102.
Shull, J. M. & Van Steenberg, M. E., 1985. *Astrophys. J.,* **294,** 599.
Shull, J. M., Snow, T. P. & York, D. G., 1981. *Astrophys. J.,* **246,** 549.
Smeding, A. G. & Pottasch, S. R., 1979. *Astr. Astrophys.,* **35,** 257.
Smith, L. F., 1968. *Mon. Not. R. astr. Soc.,* **140,** 409.
Smith, L. F., 1973. *Wolf–Rayet and High-Temperature Stars, IAU Symp. No. 49,* p. 15, eds Bappu, M. K. V. & Sahade, J., Reidel, Dordrecht, Holland.
Smith, L. F. & Kuhi, L. V., 1981. *An Atlas of Wolf–Rayet Line Profiles, JILA Rep. No. 117,* Boulder.
Smith, L. J. & Willis, A. J., 1982. *Mon. Not. R. astr. Soc.,* **201,** 451.
Smith, L. J., Willis, A. J. & Wilson, R., 1980. *Mon. Not. R. astr. Soc.,* **191,** 339.
Smith, L. J., Pettini, M., Dyson, J. & Hartquist, T. W., 1984. *Mon. Not. R. astr. Soc.,* **211,** 679.
Snow, T. P., 1980. At *ESA workshop on interstellar lines,* Vilspa, Madrid.
Spitzer, L. & Jenkins, E. B., 1975. *Ann. Rev. Astr. Astrophys.,* **13,** 133.
Strömgren, B., 1948. *Astrophys. J.,* **108,** 242.
Tarafdar, S. P., Prasad, S. S. & Huntress, W. T., 1983. *Astrophys. J.,* **267,** 156.
Van der Hucht, K. A., Conti, P. S., Lundström, I. & Stenholm, B., 1981. *Space Sci. Rev.,* **28,** 227.
Welsh, B. Y., 1983. *Mon. Not. R. astr. Soc.,* **204,** 1203.

Welsh, B. Y. & Thomas, C. K., 1982. *Mon. Not. R. astr. Soc.*, **199,** 385.
Wiese, W. L. & Fuhr, J. R., 1975. *J. Phys. Chem. Ref. Data,* **4,** 263.
Willis, A. J., 1982. *Mon. Not. R. astr. Soc.,* **198,** 897.
Willis, A. J., Howarth, I. D., Garmany, C. D. & Conti, P. S., 1986a. *Luminous Stars and Associations in Galaxies, IAU Symp. No. 116,* p. 259, eds de Loore, C. W. H., Willis, A. J. & Laskarides, P. G., Reidel, Dordrecht, Holland.
Willis, A. J., Van der Hucht, K. A., Conti, P. S. & Garmany, C. D., 1986b. *Astr. Astrophys. Suppl.,* **63,** 417.
York, D. G. & Jura, M., 1982. *Astrophys. J.,* **254,** 88.

Appendix 1: Equivalent-width errors

In this appendix we summarize the algorithms used to generate the equivalent-width errors given in Table 5; the equivalent widths themselves are calculated using trapezoidal integration. These algorithms are empirical in spirit, but we believe that they give accurate results.

We identify four sources of error:

(i) The statistical uncertainties on flux values within the line.
(ii) The statistical uncertainty in the continuum placement.
(iii) A systematic error in the continuum placement.
(iv) A systematic error in the zero level.

To begin the error analysis we define a (local) error index defined by

$$\sigma_c=\left\{\left[\sum_i\left(\frac{O_i-C_i}{C_i}\right)^2\right]\Big/N_f\right\}^{1/2}$$

where C_i is a calculated local continuum level based on a Chebyschev polynomial fit with N_f degrees of freedom. Note that by defining an error index in this way we automatically take account of any oversampling in the data.

Dealing first with source of error (i), it seems conservative (and in the case of *IUE* data, realistic) to assume that the noise is constant as a function of flux level. The error associated with each residual intensity datum in a line can be approximated by σ_c, and (assuming the data to be rectified) the corresponding fractional uncertainty on the equivalent width is simply

$$\sigma(\mathrm{i})=\sqrt{\sum_i(\Delta\lambda_i\sigma_c)^2}$$

where $\Delta\lambda$ is the wavelength spacing between points and where the summation is over points falling within the absorption feature.

The statistical error in the continuum placement – source (ii) – arises from the formal uncertainty in determining the polynomial fit coefficients which define the local continuum. The error in the (rectified) continuum placement, s_c, is of the order $\sigma_c/\sqrt{N_f}$; if the true equivalent width is given by

$$W_\lambda(T)=\sum_i\Delta\lambda_i(1-I_i)$$

then the observed equivalent width is

$$W_\lambda(O)=\sum_i\Delta\lambda_i(1+s_c-I_i)/(1+s_c),$$

[where I_i is the true residual intensity and is related to the observed value by $I_i=I_i(\mathrm{obs})\times(1+s_c)$]. Thus the fractional error on the observed equivalent width can be expressed as

$$\sigma(\mathrm{ii})=[W_\lambda(O)-W_\lambda(T)]/W_\lambda(O),$$

and a little manipulation soon gives the more useful expression

$$\sigma(\mathrm{ii})=s_{\mathrm{c}}\left[1-\frac{W_\lambda(O)}{\Delta\lambda N_L}(1+s_{\mathrm{c}})+s_{\mathrm{c}}\right]\Big/\left[\frac{W_\lambda(O)}{\Delta\lambda N_L}(1+s_{\mathrm{c}})\right],$$

where N_L is the number of points contributing to the equivalent-width measurement. (Here $\Delta\lambda$ has been taken as a constant, for clarity.) Note that for a completely saturated line the fractional error in the equivalent width due to uncertainty in the continuum placement is nil, while for a vanishingly weak line it is infinite, as intuitively expected.

In the event that the stellar spectrum is smooth and well-defined, a polynomial is likely to be a good representation of the local continuum. However, if an interstellar line lies at the bottom of a narrow stellar feature, for example, this may be far from the truth. The magnitude of the resulting error is difficult to define in an algorithmic manner, and so it seems best to proceed by subjectively estimating the maximum size of the error in locating the continuum, Δ_{c}. This error can then be propagated into an uncertainty on equivalent widths in exactly the same way as for the statistical error, s_{c}.

This leaves only (iv), a potentially important source of error for *IUE* data, particularly at the short-wavelength end of each spectrograph. We can calculate its importance much as before, by estimating the quantity Δ_0 by which the zero level may be in error in the rectified spectrum; this may be strongly wavelength-dependent in *IUE* data extracted without a background-correction algorithm, and requires careful assessment. Comparing observed and true equivalent widths we again obtain an estimate of the fractional error on the observed equivalent width

$$\sigma(\mathrm{iv})=\left[\frac{\Delta\lambda}{(1+\Delta_0)}\sum_i(1-I_i)-\Delta\lambda\sum_i(1-I_i)\right]\Big/\left[\frac{\Delta\lambda}{(1+\Delta_0)}\sum_i(1-I_i)\right].$$

The problem remains of how to combine the fractional errors, σ(i–iv), into a single value. The solution we advocate is to add them quadratically, on the grounds that any particular source of errors is as likely to decrease the difference between observed and true values as to increase it (given precautions to establish a reliable zero level, etc.); others may wish to adopt a different solution.

For data where photon statistics are relevant (some might not consider this an inadequate approximation to reduced IPCS data, for example) errors (iii) and (iv) can be treated as sketched above. One could re-define (ii) in terms of Poisson statistics, but it seems preferable to us to continue to assess it from a continuum fit. This leaves error (i); clearly it is no longer desirable to work with a constant error and residual intensities; instead we replace σ_{c} by the quantity σ_i/C_i, whence

$$\sigma(\mathrm{i})=\sqrt{\sum_i\left(\frac{\Delta\lambda}{C_i}\right)^2 n_i}$$

[where n_i is the number of counts per (independent!) channel].

Although it is difficult to construct a rigorous error analysis appropriate to equivalent-width measurements made using *IUE* data, the foregoing treatment appears to work tolerably well, and at the least has the virtue of being well defined. It is incorporated into the STARLINK DIPSO software (Howarth & Maslen 1983) which is now being widely used for the reduction of UV, optical, and IR data (e.g. Smith *et al.* 1984; McLachlin & Nandy 1985; Mountain 1985).

Appendix 2: Photoionization models

Strong lines of highly ionized species (most characteristically C IV and Si IV) are seen towards many WR stars (Smith *et al.* 1980). In the main text (Section 9.1) it was suggested that in the case

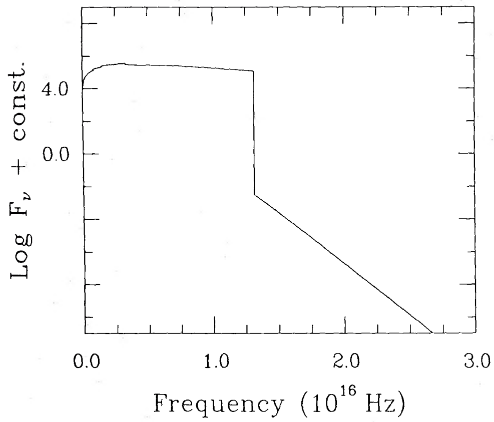

Figure A1. Flux distribution of the model atmosphere used in the H II region calculations, from Hillier (1983). The zero-point of the flux scale (in janskies) is arbitrary.

of 50896 these lines might arise in an H II region local to the WR. To see if this explanation is a plausible one we have computed a small number of exploratory models, using a photoionization code written by J. P. Harrington and made available to us in a slightly modified form by R. E. S. Clegg (see Clegg *et al.* 1986 and Harrington *et al.* 1982 for details of the computational methods and atomic data).

For simplicity we adopted a spherically symmetric geometry, and cosmic abundances as given by Snow (1980, unpublished work). A central 'hole' of radius 8 pc was assumed, to crudely simulate the swept-up region of S308; the nebula geometry is then defined by the (constant) space density of hydrogen nuclei – a free parameter – and the observed column density, $N(\mathrm{H}) = 19.6\,\mathrm{dex\,cm^{-2}}$.

The radiation field, from a model by Hillier (1983) is shown in Fig. A1. The basic model has a luminosity of $1.0\times10^5\,L_\odot$, and an effective temperature of 64 900 K; we also tried models with double and half this luminosity (at constant spectral shape). [It should be noted that the fluxes below the He II edge at 228 Å (1.3×10^{16} Hz) are incorrect even on purely numerical grounds, since the models are still optically thick at the outer boundary at these energies (J. D. Hillier,

Table A1. H II region models. Column densities in selected lines are given in units of dex $\mathrm{cm^{-2}}$. The series of models A, B, and C correspond to the basic radiation field ×1, ×2, and ×0.5; the sequences 0, 1 and 2 are for space densities of hydrogen nuclei of 1, 10, and 100 $\mathrm{cm^{-3}}$. (The A and B series are density bounded while the C series is flux bounded.)

Model	C IV	N V	Si III	Si IV	S III	S IV
Obs.	14.3	≤12.5	13.4	13.7	14.7	14.2
A0	15.8	3.4	14.6	14.7	13.9	14.6
A1	15.2	2.0	14.9	14.5	14.5	14.5
A2	13.1	...	13.2	11.6	14.5	12.6
B0	16.0	3.8	14.3	14.7	13.5	14.6
B1	15.6	2.6	14.8	14.7	14.2	14.6
B2	14.0	...	14.0	12.8	14.7	13.4
C0	15.6	2.9	14.8	14.7	14.3	14.6
C1	14.8	1.1	14.6	13.9	14.7	14.1
C2	12.2	...	12.4	10.4	14.2	11.7

personal communication). This will have a direct, and unquantifiable, effect on the calculated N^{4+} columns.]

Some results of these calculations are given in Table A1. Although we have explored only a very small parameter space, it is clear that columns as large as those observed can be obtained without too much trouble. We did not consider it worthwhile pursuing a more detailed match between the models and the observations, since (i) the heavy elements are probably depleted by an unknown amount from the gas phase, (ii) the three-dimensional geometry of the H II region is unknown, and (iii) the details of the adopted stellar fluxes are certainly wrong (e.g. no line or wind blanketing in the structure calculations, and no emission lines in the flux calculations). None the less, we believe that these calculations lend credence to the suggestion that strong lines of highly ionized species arise in regions local to 50896, and also support the view that the far-UV radiation field of this star is characterized by a rather hot effective temperature.

Note added in proof:

(1) J. Nichols-Bohlin and R. A. Fesen (*Astr. J.*, in press) give an independent discussion of the high velocity systems seen towards HD 50896, arriving at similar conclusions to those presented here.

(2) Very high dispersion ($R=10^5$) observations of the interstellar Na D lines in the spectra of many of the stars discussed in this paper support a distance of ~2 kpc for HD 50896 (W. Schmutz, I. D. Howarth, and H. Nussbaumer, in preparation).